Monthly Notices of the ROYAL ASTRONOMICAL SOCIETY

MNRAS **501,** 3640–3662 (2021) doi:10.1093/mnras/staa3690
Advance Access publication 2020 November 28

Cosmic ray driven outflows to Mpc scales from L_* galaxies

Philip F. Hopkins [1]★, T. K. Chan [2,3], Suoqing Ji [1], Cameron B. Hummels,[1] Dušan Kereš,[2] Eliot Quataert [4] and Claude-André Faucher-Giguère [5]

[1]*TAPIR, California Institute of Technology, Mailcode 350-17, Pasadena, CA 91125, USA*
[2]*Department of Physics, Center for Astrophysics and Space Science, University of California at San Diego, 9500 Gilman Drive, La Jolla, CA 92093, USA*
[3]*Institute for Computational Cosmology, Durham University, South Road, Durham DH1 3LE, UK*
[4]*Department of Astronomy and Theoretical Astrophysics Center, University of California Berkeley, Berkeley, CA 94720, USA*
[5]*Department of Physics and Astronomy and CIERA, Northwestern University, 2145 Sheridan Road, Evanston, IL 60208, USA*

Accepted 2020 November 5. Received 2020 November 4; in original form 2020 February 6

ABSTRACT

We study the effects of cosmic rays (CRs) on outflows from star-forming galaxies in the circum and intergalactic medium (CGM/IGM), in high-resolution, fully cosmological FIRE-2 simulations (accounting for mechanical and radiative stellar feedback, magnetic fields, anisotropic conduction/viscosity/CR diffusion and streaming, and CR losses). We showed previously that massive ($M_{\rm halo} \gtrsim 10^{11}\,{\rm M}_{\odot}$), low-redshift ($z \lesssim$ 1–2) haloes can have CR pressure dominate over thermal CGM pressure and balance gravity, giving rise to a cooler CGM with an equilibrium density profile. This dramatically alters outflows. Absent CRs, high gas thermal pressure in massive haloes 'traps' galactic outflows near the disc, so they recycle. With CRs injected in supernovae as modelled here, the low-pressure halo allows 'escape' and CR pressure gradients continuously accelerate this material well into the IGM in 'fast' outflows, while lower-density gas at large radii is accelerated *in situ* into 'slow' outflows that extend to >Mpc scales. CGM/IGM outflow morphologies are radically altered: they become mostly volume-filling (with inflow in a thin mid-plane layer) and coherently biconical from the disc to >Mpc. The CR-driven outflows are primarily cool ($T \sim 10^5$ K) and low velocity. All of these effects weaken and eventually vanish at lower halo masses ($\lesssim 10^{11}\,{\rm M}_{\odot}$) or higher redshifts ($z \gtrsim$ 1–2), reflecting the ratio of CR to thermal + gravitational pressure in the outer halo. We present a simple analytical model that explains all of the above phenomena. We caution that these predictions may depend on uncertain CR transport physics.

Key words: stars: formation – galaxies: active – galaxies: evolution – galaxies: formation – galaxies: intergalactic medium – cosmology: theory.

1 INTRODUCTION

Galactic outflows are ubiquitous in star-forming galaxies. Spectral observations of galaxies directly indicate outflows from the galactic interstellar medium (ISM) at a range of velocities, across a wide range of galaxy stellar masses and redshifts (Martin 1999; Heckman et al. 2000; Sato et al. 2009; Weiner et al. 2009; Martin et al. 2010; Steidel et al. 2010). Observations of the circum and intergalactic medium (CGM/IGM) also indicate that outflows must be ubiquitous in order to explain the pollution of these regions by heavy elements (Pettini et al. 2003; Songaila 2005). Moreover, it has long been recognized that outflows must occur in essentially all star-forming galaxies in order to explain their relatively low stellar masses (compared to the Universal baryon fraction) and the existence of the mass–metallicity relation (see e.g. Katz, Weinberg & Hernquist 1996; Somerville & Primack 1999; Cole et al. 2000; Springel & Hernquist 2003; Tremonti et al. 2004; Kereš et al. 2009). These outflows (primarily) stem from 'feedback' from massive stars, which can act in a variety of forms including radiative (photoheating and radiation pressure) and mechanical [thermal and kinetic energy from supernovae (SNe) explosions and outflows/jets], injection of magnetic fields and cosmic rays (CRs). In more massive galaxies, outflows from supermassive black holes (BHs) and active galactic nuclei (AGNs) are almost certainly important as well (Croton et al. 2006; Hopkins et al. 2006), but these are sub-dominant in lower-mass, star-forming galaxies (owing to the very small BHs and low duty cycle of high-accretion rate activity, among other factors; see Hopkins & Hernquist 2006, 2009; Krongold et al. 2007; Greene et al. 2011; Kormendy, Bender & Cornell 2011; Anglés-Alcázar et al. 2017).

The existence of galactic outflows in star-forming galaxies, their significance for galaxy formation and CGM/IGM evolution, and their generic attribution to 'stellar feedback' processes are well established. However, almost everything else remains controversial at some level, including e.g. the actual physical state(s) of outflowing gas (the phases/densities/temperatures/velocities that carry most of the mass/momentum/energy, and which of these if any is 'most important'), the acceleration sites (within the disc, near massive stars, or 'above the mid-plane' or in the CGM), the ultimate fate of outflows (whether they are unbound, or halt and are efficiently recycled, and if so over what time and spatial scales this occurs), their morphologies (biconical or spherical or filamentary or clumpy), and the physical feedback mechanisms that accelerate the winds (e.g. SNe versus radiation pressure versus CRs, which may act on different spatial

★ E-mail: phopkins@caltech.edu

and time-scales with different efficiencies in galaxies of different types).

In recent years, numerical simulations have begun to directly resolve the relevant scales of some of these acceleration processes in global galaxy-wide simulations, making it possible to *self-consistently* predict the *generation* of galactic winds and therefore some of the properties above (e.g. their phases and velocities), as opposed to inserting assumptions about wind properties 'by hand' (see e.g. Hopkins, Quataert & Murray 2011, 2012b; Tasker 2011; Wise et al. 2012; Agertz et al. 2013; Kannan et al. 2014; Roškar et al. 2014). One such effort is the 'Feedback In Realistic Environments' (FIRE)[1] project (Hopkins et al. 2014), which attempts to explicitly incorporate and at least begin to resolve mechanical feedback from individual SNe (Types Ia and II) as well as stellar mass-loss (O/B and AGB), following Hopkins et al. (2018b), and multiband radiation-hydrodynamics to follow photoelectric and photoionization heating and radiation pressure (Hopkins et al. 2020c), in fully cosmological simulations. These simulations have been used to explore the generation and properties of multiphase galactic outflows (Muratov et al. 2015, 2017) as well as their consequences for galactic abundances (Ma et al. 2016; Escala et al. 2018), dark matter profiles (Chan et al. 2015; Oñorbe et al. 2015), CGM absorbers around galaxies (Faucher-Giguère et al. 2016; Hafen et al. 2017, 2019, 2020), stellar haloes (El-Badry et al. 2018c; Sanderson et al. 2018), gas-phase kinematics of galaxies (Bonaca et al. 2017; Ma et al. 2017a, b; Wheeler et al. 2017; El-Badry et al. 2018a, b), and galaxy star formation (SF) histories and stellar masses (Sparre et al. 2017; Ma et al. 2018; Garrison-Kimmel et al. 2019).

Although the simulations above directly treat many of the important stellar feedback processes (e.g. SNe Types Ia and II, O/B and AGB mass-loss, photoionization and photoelectric heating, multiwavelength radiation pressure), they neglect (among other things) CRs. In the ISM, the CRs that dominate their pressure/energy density (∼GeV protons) are distributed smoothly with a $\gtrsim 1$ kpc scale-height above the disc, with order-of-magnitude similar energy densities to thermal and magnetic pressure (Ginzburg & Ptuskin 1985; Boulares & Cox 1990). The idea that this smooth 'additional pressure' term could contribute to galactic outflows by accelerating material down the CR pressure gradient if it was 'lofted' above the mid-plane (by e.g. galactic fountains) has existed for decades (Ipavich 1975; Breitschwerdt, McKenzie & Voelk 1991, 1993; Zirakashvili et al. 1996; Everett et al. 2008; Socrates, Davis & Ramirez-Ruiz 2008; Dorfi & Breitschwerdt 2012; Mao & Ostriker 2018), and in the last several years there has been a flurry of activity exploring this in numerical simulations (Jubelgas et al. 2008; Booth et al. 2013; Wiener, Zweibel & Oh 2013; Salem & Bryan 2014; Chen, Bryan & Salem 2016; Simpson et al. 2016; Ruszkowski, Yang & Zweibel 2017; Butsky & Quinn 2018; Farber et al. 2018). This work has shown not only that this is viable, but potentially consistent with a variety of observational constraints; moreover, it has also argued that this produces more 'cool' material in outflows, which can potentially enhance wind mass-loading and observable CGM absorption in certain species.

However (as is always the case), this work has limitations. Most (although not all) of the studies focused on CR winds have focused on 'idealized' simulations: either 'slabs' of a galactic disc or ISM, or isolated (non-cosmological) galaxies. This means that one cannot make meaningful predictions for the large-scale acceleration or propagation of winds beyond the immediate vicinity of the galactic disc, let alone their interaction with e.g. cosmological inflows and the high thermal pressure, virialized gaseous halo. On the other hand, the global and/or cosmological simulations that have been run have (largely owing to resolution limitations) generally treated the multiphase ISM/CGM, SF, and mechanical/radiative stellar feedback in a highly approximate fashion (in some cases ignoring these effects entirely, or not including cooling below $\sim 10^4$ K, or putting in galactic outflows 'by hand,' or simply adding SNe mechanical energy as a thermal energy component that is rapidly radiated away). In those cases, it is difficult if not impossible to self-consistently assess the impact of CR-driven outflows on different phases of gas, or their interplay with outflows driven by mechanical feedback (SNe kinetic or thermal feedback), their influence on the thermal instability, etc.

Moreover, some of the simulations above did not incorporate potentially critical CR physics: ignoring CR losses (so CRs have essentially 'infinite' energy/cooling times), treating only CR streaming or diffusion, ignoring magnetic fields (which can confine the CRs and regulate their transport), or (for numerical time-step reasons) using artificially low CR diffusion coefficients[2] $\kappa \lesssim 10^{29}\,\mathrm{cm^2\,s^{-1}}$, which artificially confines CRs near galaxies (generating stronger effects there) but violates observational constraints from spallation in the Milky Way (MW) and γ-ray emission in nearby galaxies (see Lacki et al. 2011; Cummings et al. 2016; Guo, Tian & Jin 2016; Jóhannesson et al. 2016; Korsmeier & Cuoco 2016; Fu, Xia & Shen 2017; Giacinti, Kachelrie & Semikoz 2018; Lopez et al. 2018; Chan et al. 2019). It is therefore critical to study the effects of CRs in fully cosmological simulations, which attempt to directly treat the multiphase ISM and mechanical/radiative (i.e. non-CR) stellar feedback processes, at least marginally resolve ISM structure and wind generation, and incorporate magnetic fields and anisotropic CR diffusion and streaming with transport coefficients that have been shown to reproduce observational constraints.

Working towards this goal, Chan et al. (2019) performed and presented the first simulations combining the specific physics from the FIRE simulations, described above, with explicit CR injection and transport, accounting for advection and fully anisotropic streaming and diffusion, as well as hadronic and Coulomb collisional and streaming (Alfvén) losses, and showed that for reasonable parameter choices (e.g. $\kappa \sim 10^{29-30}\,\mathrm{cm^2\,s^{-1}}$) these simulations were consistent with empirical constraints on CR propagation in the MW and nearby galaxies (both dwarf and starburst systems). In Hopkins et al. (2020d, hereafter Paper I), we presented a new large suite of >100 fully cosmological FIRE simulations incorporating these physics and the detailed physics of cooling, SF, and stellar feedback described above, in haloes from ultra-faint to >MW masses, with resolution reaching ∼pc scales. We showed that CRs produce weak effects in dwarfs and very high-redshift galaxies, but in massive ($M_{\rm halo} \gtrsim 10^{11}\,\mathrm{M_\odot}$)

[1] See the FIRE project website: http://fire.northwestern.edu

For additional movies and images of FIRE simulations, see: http://www.tapir.caltech.edu/~phopkins/Site/animations/

[2] Throughout, we will use $\kappa \equiv \kappa_\parallel$ to refer to the *parallel* diffusivity of CRs, specifically at the energies (a few GeV) that dominate the CR pressure. In many analyses of e.g. galactic CR propagation, magnetic field structure is not included so the typical value $\tilde{\kappa}_{\rm iso}$ quoted is the effective isotropic-averaged diffusivity $\tilde{\kappa}_{\rm iso} = \langle |\hat{\mathbf{B}}\cdot\hat{\nabla} e_{\rm cr}|^2\,\kappa\rangle \sim \kappa/3$ for random fields. Moreover, note that older 'leaky-box' models of the galaxy which assume CRs escape if $\gtrsim 200$ pc above the disc derive order-of-magnitude lower $\tilde{\kappa}_{\rm iso}$ compared to modern (favoured) models than allow for the existence of a diffuse gaseous halo extending ∼ 5–10 kpc above the disc, which require $\kappa \sim 3\,\tilde{\kappa}_{\rm iso} \gtrsim 3\times 10^{29}\,\mathrm{cm^2\,s^{-1}}$ (see e.g. Blasi & Amato 2012; Vladimirov et al. 2012; Gaggero et al. 2015; Cummings et al. 2016; Jóhannesson et al. 2016; Korsmeier & Cuoco 2016; Evoli et al. 2017; Amato & Blasi 2018).

haloes at $z \lesssim 2$, they can substantially suppress star formation rates (SFRs) and stellar masses. Moreover, we showed that this was primarily via their interaction with the CGM, rather than their *direct* action deep within the ISM. But in this mass and redshift range, the galaxies develop 'CR-dominated' haloes, where CRs form the dominant source of pressure support over e.g. gas thermal pressure. In Paper I and Ji et al. (2020), we followed this up and showed that a simple analytical model can predict where CRs should dominate and the ensuing equilibrium pressure and gas density profiles in CR-dominated haloes; we also showed that where CR-dominated haloes exist, they have a dramatic impact on CGM absorption statistics, and gas phase/temperature distributions. Given this and the motivation above, in this paper, we explore the effects on galactic outflows, primarily in the CGM and IGM, of these CR-dominated haloes. Indeed, we will argue that the most dramatic impact of CRs on galactic outflows occurs in the CGM and IGM, where cosmological simulations are required.

Importantly, because the micro-physics of CR transport remain highly uncertain, we assume a very simple Alfvénic streaming plus constant-parallel-diffusivity model for the CR transport parameters. In a pair of companion papers (Hopkins et al., 2020a, b), we explore more complicated models for the CR transport parameters, and show these can lead to significant differences in CGM CR pressure profiles. However, the conclusions here are generally robust *where CRs dominate the pressure*, in so far as these models are representative of reality.

In Section 2, we briefly review the numerical methods and simulation suite from Paper I. Section 3 develops and presents an analytical model for the effects of CR-dominated haloes on galactic winds. Section 4 presents our simulation results and compares them to these theoretical expectations. We review and conclude in Section 5.

2 METHODS

The specific simulations studied here are the same as those presented and studied in Paper I, where the details of the numerical methods are described. We therefore only briefly summarize here. The simulations were run with GIZMO[3] (Hopkins 2015), in its meshless finite-mass MFM mode (a mesh-free finite-volume Lagrangian Godunov method). The simulations solve the equations of ideal magnetohydrodynamics (MHD) as described and tested in Hopkins & Raives (2016) and Hopkins (2016), with fully anisotropic Spitzer–Braginskii conduction and viscosity as described in Hopkins (2017), Su et al. (2017), and Paper I (see equations 1–3 therein). Gravity is solved with fully adaptive Lagrangian force softening (so hydrodynamic and force resolutions are matched).

All our simulations include magnetic fields, anisotropic Spitzer–Braginskii conduction and viscosity, and the physics of cooling, SF, and stellar feedback from the FIRE-2 version of the FIRE project, described in detail in Hopkins et al. (2018a). Gas cooling is followed from $T = 10$–10^{10} K (including a variety of processes; e.g. metal-line, molecular, fine-structure, dust, photoelectric, photoionization cooling/heating, and accounting for self-shielding and both local radiation sources and the meta-galactic background; see Hopkins et al. 2018a). We follow 11 distinct abundances accounting for turbulent diffusion of metals and passive scalars as in Colbrook et al. (2017) and Escala et al. (2018). Gas is converted to stars using a sink-particle prescription if and only if it is locally self-gravitating at the resolution scale (Hopkins, Narayanan & Murray 2013b), self-shielded/molecular (Krumholz & Gnedin 2011), Jeans-unstable, and denser than $> 1000\,\mathrm{cm}^{-3}$. Each star particle is then evolved as a single stellar population with initial mass function (IMF)-averaged feedback properties calculated following Leitherer et al. (1999) for a Kroupa (2001) IMF and its age and abundances. We explicitly treat mechanical feedback from SNe (Ia and II) and stellar mass-loss (from O/B and AGB stars) as discussed in Hopkins et al. (2018b), and radiative feedback including photoelectric and photoionization heating and UV/optical/IR radiation pressure with a five-band radiation-hydrodynamics scheme as discussed in Hopkins et al. (2020c). Conduction adds the parallel heat flux $\kappa_{\rm cond}\,\hat{\mathbf{B}}\,(\hat{\mathbf{B}}\cdot\nabla T)$, and viscosity the anisotropic stress tensor $\Pi \equiv -3\,\eta_{\rm visc}\,(\hat{\mathbf{B}}\otimes\hat{\mathbf{B}} - \mathbb{I}/3)\,(\hat{\mathbf{B}}\otimes\hat{\mathbf{B}} - \mathbb{I}/3) : (\nabla\otimes\mathbf{v})$ to the gas momentum and energy equations, where the parallel transport coefficients $\kappa_{\rm cond}$ and $\eta_{\rm visc}$ follow the usual Spitzer & Härm (1953) and Braginskii (1965) form, accounting for saturation following Cowie & McKee (1977), and accounting for plasma instabilities (e.g. Whistler, mirror, and firehose) limiting the heat flux and anisotropic stress at high plasma-β following Komarov et al. (2018), Squire, Schekochihin & Quataert (2017c), Squire et al. (2017a), and Squire, Quataert & Kunz (2017b). The numerical implementation follows Hopkins (2017) to ensure stability. The simulations are fully cosmological 'zoom-in' runs with a high-resolution region (of size ranging from ∼1–5 Mpc on a side, increasing with $M_{\rm halo}$) surrounding a 'primary' halo of interest (Oñorbe et al. 2014).[4] The properties of these primary haloes (our main focus here, as these are the best resolved in each box) are given in Table 1. Details of all of these numerical methods are in Hopkins et al. (2018a).

Our 'CRs' or 'CR+' simulations include all of the above, and add our 'full physics' treatment of CRs as described in detail in Chan et al. (2019) and Paper I. We evolve a 'single bin' (∼GeV) or constant spectral distribution of CRs as an ultra-relativistic ($\gamma = 4/3$) fluid, accounting for injection in SNe shocks (with a fixed fraction $\epsilon_{\rm cr} = 0.1$ of the initial SNe ejecta kinetic energy in each time-resolved explosion injected into CRs), streaming and collisional (hadronic and Coulomb and ionization) losses from the CRs (accounting for local neutral fractions and composition, with a fraction of this loss thermalizing and heating gas) following Mannheim & Schlickeiser (1994) and Guo & Oh (2008), advection and adiabatic work (in the local 'strong coupling' approximation, so the CR pressure contributes to the total pressure in the Riemann problem for the gas equations-of-motion), and CR transport including fully anisotropic diffusion and streaming (McKenzie & Voelk 1982). We solve the transport equations using a two-moment approximation to the collisionless Boltzmann equation (with a 'reduced speed of light' $\tilde{c} \sim 1000\,\mathrm{km\,s^{-1}}$), with a constant parallel diffusivity $\kappa_{\parallel}$ (perpendicular $\kappa_{\perp} = 0$). The streaming velocity is $\mathbf{v}_{\rm stream} = -v_{\rm stream}\,\hat{\mathbf{B}}\,(\hat{\mathbf{B}}\cdot\hat{\nabla}P_{\rm cr})$ with $v_{\rm stream} = 3\,v_{\rm A}$ ($v_{\rm A}$ the Alfvén speed) our default choice, motivated by models favouring trans or modestly super-Alfvénic streaming (Skilling 1971; Holman, Ionson & Scott 1979; Kulsrud 2005; Yan & Lazarian 2008), although varying this widely (from $< 1\,v_{\rm A}$ to $\sim 3\,(c_s^2 + v_{\rm A}^2)^{1/2} \gg v_{\rm A}$) has almost no effect on our conclusions (see Paper I). The 'streaming loss' term $\mathbf{v}_{\rm A}\cdot\nabla P_{\rm cr}$ represents losses to plasma instabilities at the CR gyro scale and is thermalized (Wentzel 1968; Kulsrud & Pearce 1969).

Our 'baseline' or 'no CRs' simulations include all the physics above except CRs: these are the 'MHD+' simulations in Paper I. Note there we also compared a set without magnetic fields, conduction,

[3]A public version of GIZMO is available at http://www.tapir.caltech.edu/~phopkins/Site/GIZMO.html.

[4]For the MUSIC (Hahn & Abel 2011) files necessary to generate all ICs here, see: http://www.tapir.caltech.edu/~phopkins/publicICs

Table 1. Zoom-in simulation volumes run to $z = 0$ (see Hopkins et al. 2018a for details). All units are physical.

Simulation Name	$M_{\rm halo}^{\rm vir}$ ($M_\odot$)	$M_*^{\rm MHD+}$ ($M_\odot$)	$M_*^{\rm CR+}$ ($M_\odot$)	$m_{i,\,1000}$ ($1000\,M_\odot$)	$\langle\epsilon_{\rm gas}\rangle^{\rm sf}$ (pc)	Notes
m09	2.4e9	2e4	3e4	0.25	0.7	early-forming, ultra-faint field dwarf
m10v	8.3e9	2e5	3e5	0.25	0.7	isolated dwarf in a late-forming halo
m10q	8.0e9	2e6	2e6	0.25	0.8	isolated dwarf in an early-forming halo
m10y	1.4e10	1e7	1e7	0.25	0.7	early-forming dwarf, with a large dark matter 'core'
m10z	3.4e10	4e7	3e7	0.25	0.8	ultra-diffuse dwarf galaxy, with companions
m11a	3.5e10	6e7	5e7	2.1	1.6	classical dwarf spheroidal
m11b	4.3e10	8e7	8e7	2.1	1.6	discy (rapidly rotating) dwarf
m11i	6.8e10	6e8	2e8	7.0	1.8	dwarf with late mergers and accretion
m11e	1.4e11	1e9	7e8	7.0	2.0	low-surface brightness dwarf
m11c	1.4e11	1e9	9e8	2.1	1.3	late-forming, LMC-mass halo
m11q	1.5e11	1e9	1e9	0.88	1.0	early-forming, large-core diffuse galaxy
m11v	3.2e11	2e9	1e9	7.0	2.4	has a multiple-merger ongoing at $z \sim 0$
m11h	2.0e11	4e9	3e9	7.0	1.9	early-forming, compact halo
m11d	3.3e11	4e9	2e9	7.0	2.1	late-forming, 'fluffy' halo and galaxy
m11f	5.2e11	3e10	1e10	12	2.6	early-forming, intermediate-mass halo
m11g	6.6e11	5e10	1e10	12	2.9	late-forming, intermediate-mass halo
m12z	8.7e11	2e10	8e9	4.0	1.8	disc with little bulge, ongoing merger at $z \sim 0$
m12r	8.9e11	2e10	9e9	7.0	2.0	late-forming, barred thick-disc
m12w	1.0e12	6e10	2e10	7.0	2.1	forms a low-surface brightness / diffuse disc
m12i	1.2e12	7e10	3e10	7.0	2.0	'Latte' halo, later-forming MW-mass halo, massive disc
m12b	1.3e12	9e10	4e10	7.0	2.2	early-forming, compact bulge + thin disc
m12c	1.3e12	6e10	2e10	7.0	1.9	MW-mass halo with $z \sim 1$ major merger(s)
m12m	1.5e12	1e11	3e10	7.0	2.3	earlier-forming halo, features strong bar at late times
m12f	1.6e12	8e10	4e10	7.0	1.9	MW-like disc, merges with LMC-like companion

Note. Halo/stellar properties listed refer only to the original 'target' halo around which the high-resolution volume is centred: these volumes can reach up to $\sim$ (1–10 Mpc)^3 comoving, so there are actually several hundred resolved galaxies in total. **(1)** Simulation Name: Designation used throughout this paper. **(2)** $M_{\rm halo}^{\rm vir}$: Virial mass (following Bryan & Norman 1998) of the 'target' halo at $z = 0$. **(3)** $M_*^{\rm MHD+}$: Stellar mass of the central galaxy at $z = 0$, in our non-CR, but otherwise full-physics ('MHD+') run. **(4)** $M_*^{\rm CR+}$: Stellar mass of the central galaxy at $z = 0$, in our 'default' (observationally favoured) CR+ ($\kappa = 3e29$) run. **(5)** $m_{i,\,1000}$: Mass resolution: the baryonic (gas or star) particle/element mass, in units of $1000\,M_\odot$. The DM particle mass is always larger by the universal ratio, a factor $\approx$5. **(6)** $\langle\epsilon_{\rm gas}\rangle^{\rm sf}$: Spatial resolution: the gravitational force softening (Plummer-equivalent) at the mean density of SF (gas softenings are adaptive and match the hydrodynamic resolution, so this varies), in the MHD+ run. Typical time resolution reaches $\sim$ 100–100 yr, density resolution $\sim 10^3$–10^4 cm^{-3}. **(7)** Additional notes.

or viscosity (the 'Hydro+' runs); but as shown therein and in Su et al. (2017) the differences in these runs are largely negligible, and we confirm this here. Our default 'CR' simulations adopt $\kappa_\parallel = 3 \times 10^{29}$ cm^2 s^{-1}, along with the full physics of anisotropic streaming, diffusion, collisional losses, etc., above: these are the 'CR+($\kappa = 3e29$)' simulations in Paper I. Although we considered variations to all of these CR physics and, in particular, the diffusivity (which is not known a priori) in Paper I, we showed that the observational constraints from e.g. spallation and more detailed measurements in the MW and γ-ray emission in local galaxies were all consistent with the default ($\kappa_\parallel = 3 \times 10^{29}$ cm^2 s^{-1}) model here, and ruled out models (within the context of the approximations here) with much lower/higher $\kappa_\parallel$.

3 THEORETICAL EXPECTATIONS

In Paper I, we developed a simple toy model for 'CR-dominated haloes,' and in Paper I and Ji et al. (2020) we validated this as a surprisingly accurate description of the CR pressure and density profiles in the CGM of our simulations. We therefore apply it here to outflows.

Although there has been significant study of CR-driven outflows 'within' or 'just outside' galaxies (i.e. within ~ 1 kpc 'off' the vertical surface of a thin disc, which we will study in detail in Chan et al., in preparation), we will argue below that many (not all) of the most dramatic differences owing to CRs occur on much larger scales in the CGM and IGM. Therefore on these scales, we can approximate the galaxy as small, so the injection of CRs is point-like, with quasi-steady rate $\dot{E}_{\rm cr} = \epsilon_{\rm cr}\,\dot{E}_{\rm SNe} = \epsilon_{\rm cr}\,u_{\rm SNe}\,\dot{M}_*$, averaged at a given radius over the CR diffusion time to that point ($\sim$Gyr). For the cases of interest, the CRs have some effective (isotropic-averaged) diffusivity $\tilde{\kappa}$ (which Ji et al. 2020 and Paper I argued should be $\sim\kappa_\parallel/3$), and escape the galaxy with negligible collisional losses (requiring $\tilde{\kappa} \gtrsim 10^{29}$ cm^2 s^{-1} in MW-like and dwarf galaxies; see Chan et al. 2019 and Paper I). The CRs quickly form a spherically symmetric radial pressure profile with $P_{\rm cr} \approx \dot{E}/(12\pi\,\tilde{\kappa}\,r)$ at $r < r_{\rm stream}$ and $P_{\rm cr} \approx \dot{E}/(12\pi\,v_{\rm stream}\,r^2)$ at $r > r_{\rm stream}$, with $r_{\rm stream} \equiv \tilde{\kappa}/v_{\rm stream} \sim \tilde{\kappa}/v_{\rm A}(r_{\rm stream})$.

The case of particular interest is where this *dominates* over thermal pressure in the CGM. As discussed in Paper I, for this to be the case, it requires $P_{\rm cr} \gtrsim P_{\rm thermal,\,vir} \sim (3/16)\,200\,\bar{\rho}\,V_{\rm vir}^2$, or $\dot{E}_{\rm cr}/10^{41}\,{\rm erg\,s^{-1}} \gtrsim 1.7\,\tilde{\kappa}_{29}\,M_{\rm halo,\,12}\,(1+z)^3$. Assuming CRs from SNe with $\epsilon_{\rm cr} = 0.1$ and our adopted IMF, with time-averaged SFRs $\dot{M}_* \equiv \alpha\,M_*(z)/t_{\rm Hubble}(z)$ ($\alpha \sim 1$), this is equivalent to $P_{\rm cr}/P_{\rm vir} \approx 3\,(1+z)^{-3/2}\,(M_*/f_{\rm baryon}\,M_{\rm halo})\,\alpha\,\tilde{\kappa}_{29}^{-1}$, so we expect (as we showed in Paper I) the haloes are only CR-dominated at redshifts $z \lesssim 1$–2, in the mass range $M_{\rm halo} \gtrsim 10^{11-13}\,M_\odot$ where $M_*/f_{\rm baryon}\,M_{\rm halo}$ is relatively large.

In this regime, following Ji et al. (2020), if we take $P = P_{\rm total} \approx P_{\rm cr}$ (since, by definition, CRs dominate the pressure), we can

compare the outward pressure gradient force to the gravitational force $\rho\,\partial\Phi/\partial r$, and we immediately see there is a critical density $\rho_{\rm crit}$ where the two are equal, $\rho_{\rm crit} \approx \dot{E}_{\rm cr}/(12\pi\,V_c^2\,\tilde{\kappa}\,r)$ at $r \ll r_{\rm stream}$ and $\rho_{\rm crit} \approx \dot{E}_{\rm cr}/(6\pi\,V_c^2\,v_{\rm stream}\,r^2)$ at $r \gg r_{\rm stream}$. We can approximate V_c with a Hernquist (1990) profile ($\Phi \sim -G\,M_{\rm halo}/(r+2\,r_s)$) or NFW profile where r_s is the usual NFW scale radius $=R_{\rm vir}/c$ with $c \approx 10$ at $z=0$.[5] If we define $V_0 = \sqrt{G\,M_{\rm halo}/r_s}$, this gives $\rho_{\rm crit} \sim 0.07\,\dot{E}_{\rm cr}\,r_s/(V_0^2\,\tilde{\kappa}\,r^2)$ at small r and $\rho_{\rm crit} \sim 0.04\,\dot{E}_{\rm cr}/(V_0^2\,v_{\rm stream}\,r_s\,r)$ at large r. Regardless of V_c, with no other forces, at any r, gas with $\rho < \rho_{\rm crit}$ will rise (move outwards) while gas with $\rho > \rho_{\rm crit}$ will sink (infall).

3.1 Global, steady-state wind solutions

First for simplicity, consider steady-state (time-independent), global, spherically symmetric outflow solutions of the Euler-equations, in a CR-dominated halo (so $P = P_{\rm cr}$), with no other forces other than gravity (determined by the dark matter, so ignoring self-gravity of the outflow). From continuity, we have $v_r = \dot{M}_{\rm out}/(4\pi\,\rho\,r^2)$. The momentum equation can then be written $(\dot{M}_{\rm out}/4\pi\,\rho\,r^2)^2\,(2 + d\ln\rho/d\ln r) + \rho^{-1}\,dP_{\rm cr}/d\ln r + V_c^2 = 0$. Inserting $P_{\rm cr} \approx \dot{E}/(12\pi\,\tilde{\kappa}\,r\,[1 + r/r_{\rm stream}])$ (which interpolates between the regimes $r \gg r_{\rm stream}$ and $r \ll r_{\rm stream}$ above), it is easy to verify numerically that this has a continuum of smooth outflow solutions. The resulting density and radial velocity profiles are monotonically decreasing with r, positive definite, continuous and infinitely differentiable.

At small/intermediate radii $r \lesssim {\rm MIN}\,((r_{\rm stream}, r_s))$, the solutions asymptote to $\rho \rightarrow \rho_{\rm crit}$ and $v_r \rightarrow (G\,M_{\rm halo}\,\tilde{\kappa}\,\dot{M}_{\rm out})/(r_s^2\,\dot{E}_{\rm cr}) \sim$ constant. Using $\epsilon_{\rm cr} = 0.1$, our adopted IMF, the relation between r_s and $R_{\rm vir}$ for haloes with concentration $\sim$10, and the fact that $\dot{E}_{\rm cr} = \epsilon_{\rm cr}\,u_{\rm SNe}\,\dot{M}_*$ (with $\dot{M}_* = \alpha\,M_*/t_{\rm Hubble}$), we can rewrite this as: $\dot{M}_{\rm out}/\dot{M}_* \sim 0.6\,(1+z)^{-2}\,(v_r/10\,{\rm km\,s^{-1}})$, $(\Delta\Omega/4\pi)\,\tilde{\kappa}_{29}^{-1}\,(M_{\rm halo}/10^{12}\,{\rm M_\odot})^{-1/3}$where $\Delta\Omega$ is the solid angle covered by the outflow (assuming a constant-$\Delta\Omega$ geometry). Outflow solutions exist, and they allow for arbitrarily small outflow velocity (albeit with small associated $\dot{M}_{\rm out} \propto v_r$, as well). Along different sightlines/solid angles, one can have different central v_r corresponding to different outflow rates along that angle (e.g. the bipolar winds we will see below). At large radii in the outflow ($r \gtrsim {\rm MAX}(r_{\rm stream}, r_s)$), ρ and v_r gradually decline as $\sim 1/r$ (decreasing monotonically from their values at small r).

3.2 Non-steady-state inflow/outflow behaviour

Consider a parcel of gas with initial density ρ_i at some radius r in the CR-dominated halo described above. If $\rho_i \neq \rho_{\rm crit}$, it experiences a non-zero net acceleration.

For $\rho_i \gg \rho_{\rm crit}$, the dominant term in the equation of motion is the gravitational acceleration, so the parcel (at least initially) essentially free-falls on to the galaxy. If we imagine a small (but finite)-sized parcel with all its mass free-falling on pure-radial trajectories (so the solid angle subtended by the parcel is conserved), with an initial radial thickness Δr, then as it falls in it will be compressed in the tangential direction but tidally stretched,[6] so $\rho \propto r^{-\alpha}$ with $\alpha \approx 2$ at $r \ll r_s$ and $\alpha \approx 3/2$ at $r \gg r_s$. At small $r_i \ll r_s$, since $\rho_{\rm crit} \propto r^{-(1\,-\,2)}$ (depending on how κ and $v_{\rm st}$ scale), this means the ratio $\rho/\rho_{\rm crit}$ is conserved or increases as the parcel falls towards the galaxy, allowing it to fall 'through' to the galaxy. But if the parcel is initially moving slowly at large r (where $\rho_{\rm crit} \propto r^{-(3\,-\,4)}$) its density increases more slowly than $\rho_{\rm crit}$ as it falls in, so it will eventually decelerate and halt.

For $\rho_i \ll \rho_{\rm crit}$, the dominant term is outward acceleration by CRs, so the parcel is accelerated into outflow. If we make the same geometric assumptions as above, then the 'tidal' force from $P_{\rm cr}$ on a parcel or shell is compressive, and $\rho \sim$constant as the shell is accelerated at small r_i or $\rho \propto r$ at large r_i. This means the acceleration from CRs becomes weaker as the parcel accelerates and is dominated by the acceleration near r_i. Eventually, $\rho/\rho_{\rm crit}$ increases and the gravitational force will again become comparable to or dominate CR acceleration; however, if the parcel has already been accelerated to very large $v_r \gtrsim V_c$, it can travel 'ballistically' a large distance or even escape. For the assumptions above, the acceleration near r_i is quasi-impulsive (relative to the outflow time-scale), and accelerates a parcel to a local 'terminal' $v_r \rightarrow \sqrt{2}\,V_c(r_i)\,(\rho_{\rm crit}/\rho_i - 1)^{1/2}$ for small r_i or $v_r \rightarrow \sqrt{2}\,V_c(r_i)\,([\rho_{\rm crit}/\rho_i - 1]/3)^{1/2}$ for large r_i.

So *if* some local process (e.g. ejection of low-density wind material from the galactic disc, or rarefactions in a turbulent halo) can generate gas with $\rho_i \ll \rho_{\rm crit}$ at a given radius, it will rapidly be accelerated to velocities of the order of the circular or escape speed, $\sim V_c\,(\rho_i/\rho_{\rm crit})^{-1/2}$ and can travel to very large radii or be unbound.

3.3 Wind 'trapping' or pressure confinement

Above we considered free expanding/contracting solutions. If the galactic disc impulsively ejects some gas, we should also consider the role of the gas column 'above' it potentially confining these outflows.

3.3.1 Gas pressure-dominated halos (weak CRs)

First, consider the case *without* CRs. Assume the 'initial' halo is in hydrostatic equilibrium with gas pressure following a $P = P_0\,(\rho/\rho_0)^{5/3}$ adiabat[7] inside $R < R_{\rm vir}$ in a Hernquist (1990) profile halo with $c = 10$, and that the universal baryon fraction $f_{\rm baryon}\,M_{\rm halo}$ is in gas inside $R_{\rm vir}$ (with $P = (3/16)\,\rho\,V_{\rm vir}^2$ just inside $R_{\rm vir}$, appropriate for the post-virial-shock gas). This implies a gas pressure $P = P_0\,(\Psi/(1 + r/2\,r_s))^{5/2}$ where $\Psi \approx 0.2\,G\,M_{\rm halo}\,\rho_0/r_s\,P_0$. If a spherical outflow moves out of the disc, there is an energetic cost ΔE associated with the 'PdV' work of 'lifting' this column. This can easily be integrated from $r = 0$ to r, to show at small $r \lesssim a$, $\Delta E = \int P\,{\rm d}V \approx P(r=0)\,(4\pi\,r^3/3)$, or for a wind expanding at some $v_{\rm wind} = v_r$, $\dot{E}_{\rm work} \approx P_0\,(2\,\Psi/3)^{5/2}\,8\pi\,r^2\,v_r$. If we use the normalization conditions above to solve for P_0 and ρ_0, and equate this to a constant energy-injection rate $\dot{E}_{\rm wind} \approx (1/2)\,\dot{M}_{\rm out}\,v_{\rm wind}^2$, we find that the wind should 'stall' relatively quickly as the energetic cost of pushing further at $v_{\rm wind}$ becomes larger than the energy

[5] We obtain very similar results assuming a Hernquist (1990) or NFW profile (at all $r \lesssim 100\,r_s$), but some of the expressions below must be evaluated numerically for NFW (or have weakly varying logarithmic corrections) so we default to the expressions for a Hernquist (1990) for simplicity.

[6] Of course the 'deformation' of a parcel and its density evolution will be sensitive to other terms such as magnetic tension and ram pressure. In our simulations, these terms are generally small compared to the CR and tidal forces so we neglect them in our simple analytical argument. If we had much lower CR pressure, we of course revert to behaviour more akin to classic multiphase accretion/CGM models relevant in the 'no CRs' limit. But more detailed study in idealized simulations like those in Butsky et al. (2020) is warranted.

[7] Assuming instead some power-law entropic function $P/\rho^{5/3} \propto r^n$ with $n \sim$ 0–1, as suggested in e.g. Stern et al. (2019) for quasi-hydrostatic cooling-flow haloes, only changes our argument here by an order-unity coefficient.

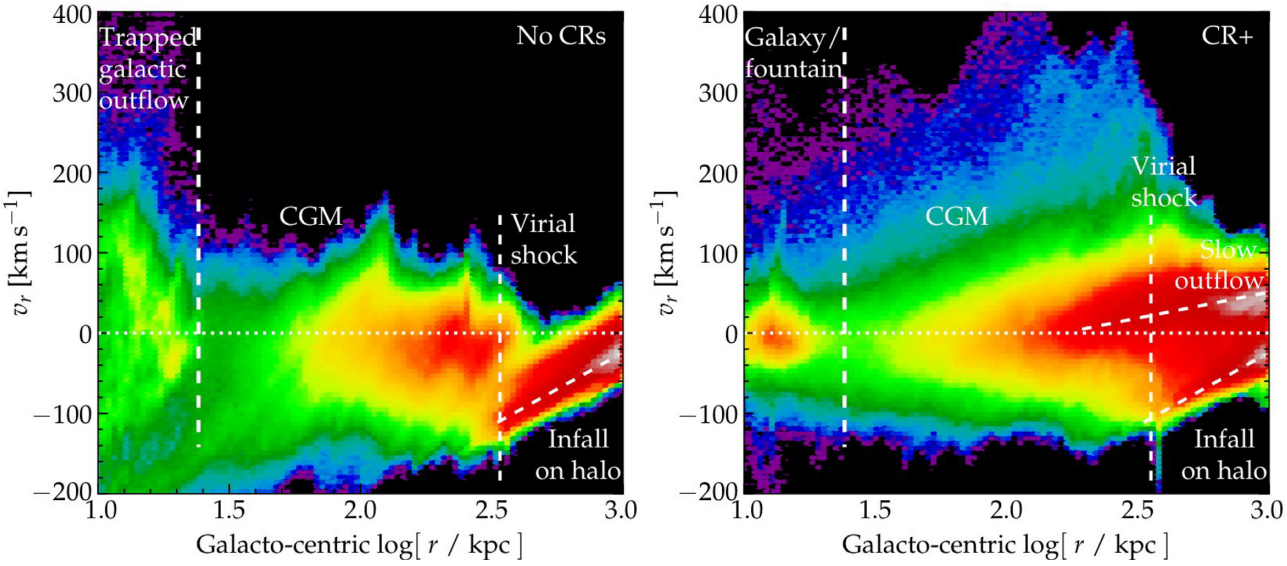

Figure 1. Distribution of gas radial inflow (negative) or outflow (positive) velocities v_r in our halo **m12i** (at $z = 0$) – a case study where the effects of CRs are most dramatic. We compare runs without CRs ('No CRs' or 'MHD+'; *left*) and with CRs ('CR+' or 'CR+($\kappa = 3e29$)'; *right*), as a function of galactocentric distance r. Colours show (logarithmically scaled) mass-weighted density in the plot (increasing purple-to-white). We label some components: (a) gas infalling from $\gtrsim 1$ Mpc to $\sim R_{\rm vir}$ at (roughly) free-fall velocities; (b) the virial radius, where a strong shock is evident in the 'No CRs' run (v_r 'jumping' to $\sim$0); (c) the CGM; (d) the 'outer galaxy' or 'fountain' regime ($\lesssim 30$ kpc). Absent CRs (still including MHD, conduction, radiation-hydrodynamics, stellar feedback, etc.), outflows are trapped by large halo thermal pressure, stirring large velocities in the disc. With CRs (for the parameters here, which have a near-maximal effect), CR pressure continuously accelerates material past $\gtrsim 10$ kpc, and the low-thermal-pressure halo allows it to escape easily, producing fast outflows to $\sim R_{\rm vir}$, and 'slow' ($< 100\,{\rm km\,s^{-1}}$) outflows accelerated *in situ* by CRs at ~ 0.5–$5\,R_{\rm vir}$.

injection rate in the wind, with the 'stalling radius' just $\sim 10\,{\rm kpc}\,(1+z)^{-2}\,M_{\rm halo,\,12}^{-1/3}\,\left(\dot{M}_{\rm out}\,v_{\rm wind}/{\rm M_\odot\,yr^{-1}}\,500\,{\rm km\,s^{-1}}\right)^{1/2}$. In other words, even winds launched fairly 'violently' (with $v \gtrsim 500\,{\rm km\,s^{-1}}$ and $\dot{M}_{\rm out} \gtrsim {\rm M_\odot\,yr^{-1}}$) will stall quickly (at ~ 10 kpc), unless they involve extremely large momentum fluxes (usually seen only in AGN-driven winds).

Of course, it is possible for winds to escape without stalling if they do not entrain the gas but 'punch through' the hot halo – e.g. if dense clumps or filaments, with small covering factor, are ejected from the disc. These would move ballistically, at least initially, although secondary Kelvin–Helmholtz or Rayleigh–Taylor instabilities should generally 'shred' such clouds fair quickly in a hot halo and mix them efficiently.

3.3.2 *CR-pressure dominated halos*

In the other hand, in the CR-dominated regime, where the pressure primarily comes from CRs, then if the halo gas is primarily sitting at $\rho \approx \rho_{\rm crit}$, and has a much lower temperature set by photoionization equilibrium rather than hydrostatic pressure equilibrium, the gas thermal pressure is essentially negligible. If we assume $\rho(r) \sim \rho_{\rm crit}(r) = \dot{E}_{\rm cr}/(12\pi\,V_c^2\,\tilde{\kappa}\,r)$ and $T \sim 10^5\,{\rm K}$ at all radii (using the more exact expression assuming photoionization equilibrium makes little difference), then calculate $\dot{E}_{\rm work} \sim P\,{\rm d}V/{\rm d}t \sim 4\pi\,P\,r^2\,v_{\rm wind}$ and compare this to the energy injection rate $\dot{E}_{\rm wind} \approx (1/2)\,\dot{M}_{\rm out}\,v_{\rm wind}^2$, we find that a disc-launch wind would be sufficient to provide the 'PdV' work required to lift the cool (low-pressure) CR dominated gaseous halo to $r \rightarrow \infty$ for $v_{\rm wind}\,(\dot{M}_{\rm out}/\dot{M}_*) \gtrsim 30\,{\rm km\,s^{-1}}\,\tilde{\kappa}_{29}^{-1}\,M_{\rm halo,\,12}^{-1/3}$.

What is important here is that a similar 'PdV' work is *not* required to 'lift' the CR fluid. Because the CRs are diffusive, with diffusion time on $\sim$ 1–10 kpc scales $\sim$ 1–100 Myr much faster than the wind expansion time, the CRs simply diffuse *through* the outflowing gas, maintaining the equilibrium CR energy density/pressure profile essentially *independent* of the wind. In other words, CRs are not efficiently 'entrained,' let alone 'compressed' by these outflows. This means that the gas can gain the benefit of CR acceleration, by feeling the quasi-static CR pressure gradient on large length scales $\sim r$, but does not have to work against the CRs when escaping.

This means that *dense* outflows from the disc will behave more-or-less ballistically, in the halo, and can escape or reach much larger radii before recycling. Moreover, low-density outflows with $\rho_i \ll \rho_{\rm crit}$ will be further accelerated in a CR-dominated halo, as described above. In fact, the steady-state solutions above show that, for gas with $\rho \lesssim \rho_{\rm crit}$, there is effectively no 'escape velocity' – steady-state outflow solutions reaching $r \rightarrow \infty$ and carrying constant $\dot{M}_{\rm out}$ exist for *arbitrarily* low initial wind $v_{\rm wind} = v_r$.

4 RESULTS

4.1 Case study of a Milky Way-mass, low-redshift halo

We first consider a 'case study' of halo **m12i** at redshift $z \sim 0$. This is instructive because it will allow us to test the analytical theory in Section 3, and demonstrate essentially all of the qualitative features imprinted on outflows in our broader survey. We select halo **m12i**: as an MW-mass halo (and at present-day $z \sim 0$), this lies at the 'sweet spot' where the effects of CRs from SNe are near-maximal on essentially all properties studied here or in Paper I. Here $M_*/M_{\rm halo}$ is maximized, so the magnitude of CR pressure relative to virial in the halo is largest, but the galaxy still allows most of the CRs to escape the dense star-forming disc gas without losses (see Paper I and Chan et al. 2019 for extensive discussion).

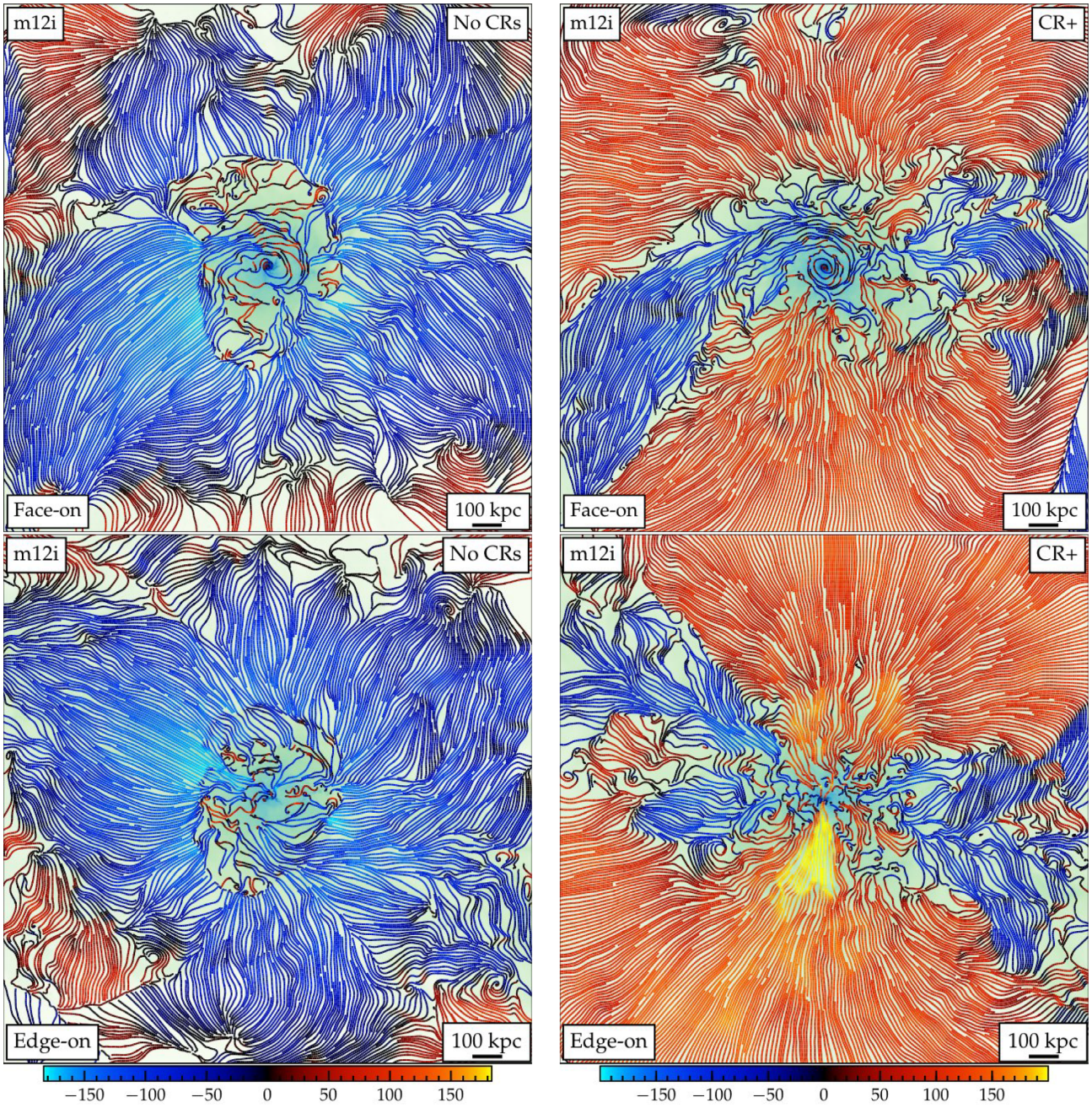

Figure 2. Inflow/outflow structure in **m12i**, runs without CRs (*left*) and with CRs (*right*). We plot gas velocity (**v**) streamlines, in a 2D slice (background colour shows gas density, to indicate the disc location in cyan). Lines are coloured by radial velocity v_r in km s^{-1} (see colour bar: red is outflow, blue is inflow). We compare face-on (*top*) and edge-on (*bottom*) projections (with respect to the galactic disc plane), in a box with extending to ± 1 Mpc ($\approx 8\,R_{\rm vir}$ across) away from the galaxy centre in both directions (see scale bar). The CR run exhibits qualitatively different structure: 'No CRs' (MHD+) shows inflow in all directions from the cosmic web on to a very obvious/sharp virial shock at ~ 250 kpc, with a turbulent, inflow-dominated halo interior to this. 'CR+' shows inflow penetrating in the mid-plane and filament feeding the disc, with strong bipolar outflow filling almost all the large-scale volume to >Mpc scales.

We will compare the two 'baseline' simulations: 'No CRs' or 'MHD+' from Paper I (all physics of SF, stellar feedback, MHD, conduction, viscosity, but no CRs) and 'CR+' or 'CR+($\kappa = 3e29$)' from Paper I (which has parameters for CRs favoured observationally and theoretically, and produces the maximal effect of our CR runs); see Section 2. First, we consider several 'snapshots' of the gas inflow/outflow properties at $z = 0$. Fig. 1 shows the distribution of gas inflow and outflow velocities in the disc/galactic fountain regime, CGM, and IGM. Figs 2–3 show streamlines of the inflow/outflow on scales $R_{\rm vir}$ and $\gg R_{\rm vir}$. Fig. 4 shows the total mass inflow and outflow rates at different radii, as well as the flux-weighted mean velocities of the inflowing and outflowing gas. Fig. 5 examines the phase structure of the outflows in more detail, specifically correlations between gas density, temperature, and outflow/inflow velocities, in the CGM/IGM gas, while Fig. 6 follows the histories of gas parcels as they are accelerated into outflow. Fig. 7 more quantitatively assesses the outflow geometry (polar-angle dependence).

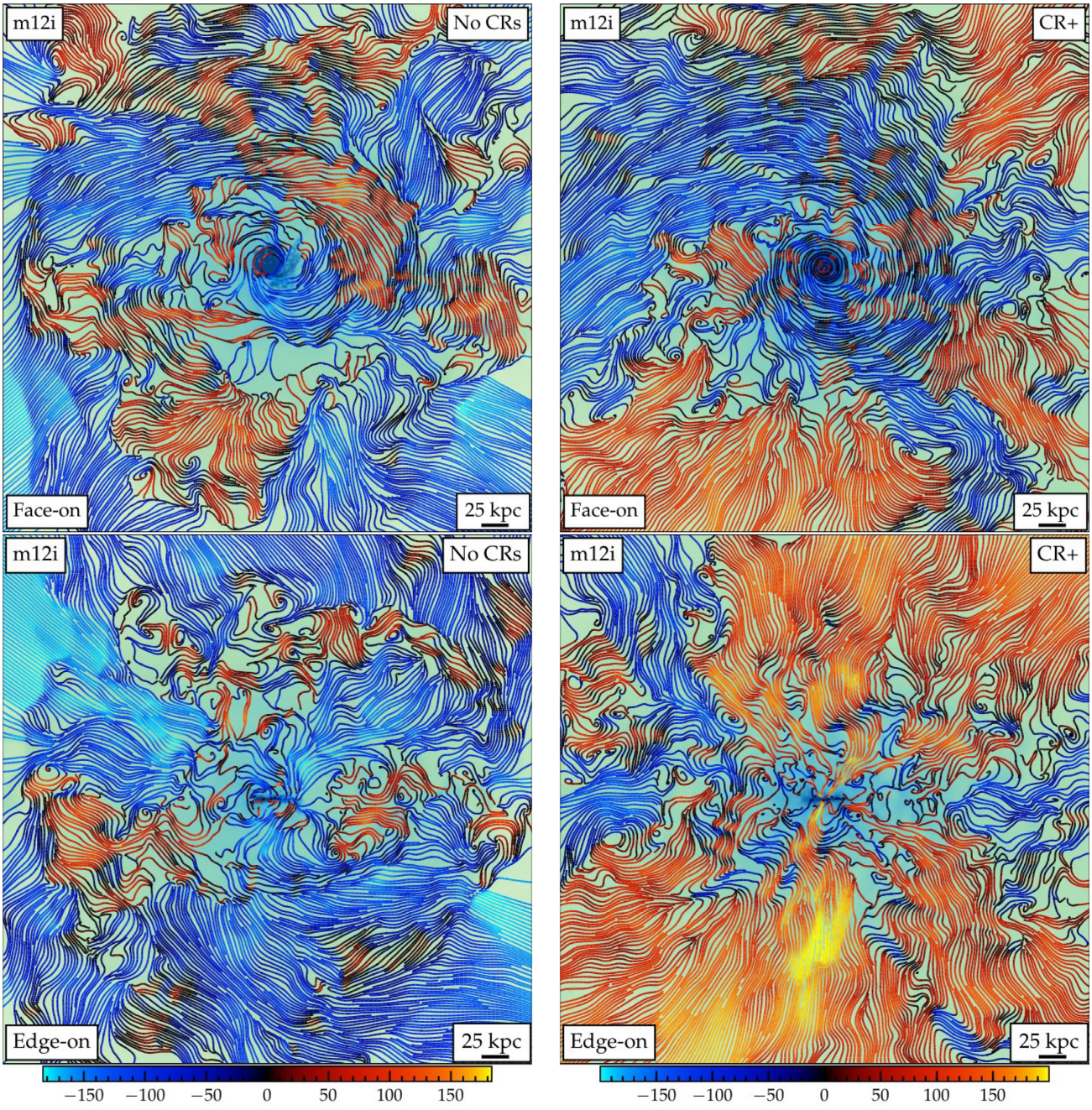

Figure 3. Inflow/outflow as Fig. 2, but zooming in to a smaller box at about the radius of the virial shock in the 'No CRs' run (side-length $\pm 1\ R_{\rm vir}$; see scale bar). The qualitative difference between CR and non-CR runs persists, but is less dramatic. We still see substantial turbulence in the inflowing gas for the non-CR run, and more similar mid-plane structure of inflowing gas in both runs (the primary difference is the bipolar outflows, which extend down to the disc).

4.1.1 Outflow kinematics and acceleration

From these, we immediately see a number of striking differences with CRs. The CR+ run features a CR pressure-dominated halo, as expected for this mass and redshift range, which (owing to rapid CR diffusion) is well approximated by a simple spherically symmetric equilibrium model (see Section 3 and Paper I). This, in turn, predicts a simple equilibrium density $\rho_{\rm crit} \equiv |{\rm d}P_{\rm cr}/{\rm d}\ln r|/V_c^2$ at each radius, where CR pressure balances gravity, and indeed where most of the gas appears to reside (see Ji et al. 2020). Lower-density material has a net outward acceleration ($a_{\rm cr} \propto \rho^{-1}\,{\rm d}P_{\rm cr}/{\rm d}r$ outward, larger than the gravitational $a_{\rm grav} \propto V_c^2/r$ inward), and appears to be re-accelerated at each r up to the expected terminal velocity for its density (Section 3), giving rise to both 'fast' and 'slow' outflows at large $R \sim 0.5$–$5\ R_{\rm vir}$.

Moreover, if anything, Figs 1 and 4 show that without CRs, outflows *within and around* the disc ($r \lesssim 30$ kpc) actually have slightly *larger* mass-loading $\dot{M}_{\rm out}/\dot{M}_*$ (and recall, the run without CRs has a $\sim$2.5 $\times$ higher SFR, so the absolute $\dot{M}_{\rm out}$ is correspondingly larger), and significantly larger velocities ($> 100\,{\rm km\,s^{-1}}$). But without CRs, the outflow rate drops precipitously at larger radii, while with CRs,

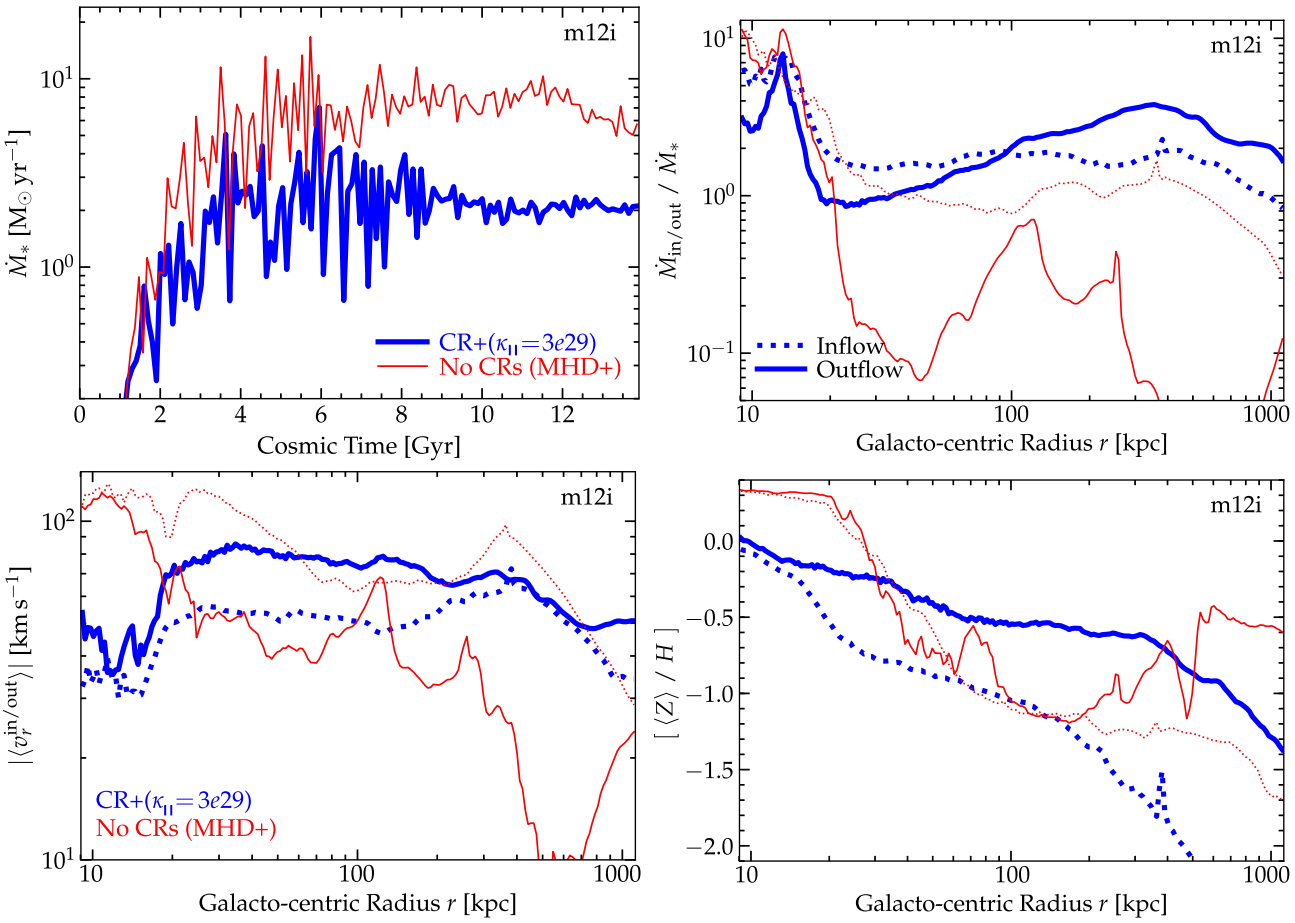

Figure 4. Basic SF and inflow/outflow properties in **m12i**. *Top left:* SFR ($\dot{M}_*$) versus cosmic time. Including CRs from SNe, SFRs in MW-mass haloes are significantly suppressed below $z\sim1$–2 (see Paper I). *Top right:* Inflow (*dotted*) and outflow (*solid*) rates through each radial annulus at $z=0$ (normalized to the SFR). Note inflow + outflow co-exist because the flow is not spherically symmetric. *Bottom left:* Inflow and outflow $\dot{M}_{\rm in/out}$-weighted mean radial velocities $\langle v_r\rangle$ in or out, versus radius at $z=0$. *Bottom right:* Inflow and outflow $\dot{M}_{\rm in/out}$-weighted metallicities [Z/H] $=\log_{10}(\langle Z\rangle/Z_\odot)$. Gross inflow rates $\dot{M}_{\rm in}$ on to the halo (at $\gtrsim R_{\rm vir}$) are similar (more so in absolute units), indicating most of the inflow comes in the dense planar structures that remain in the 'CR+' run (Fig. 2); but inflows accelerate to larger $\langle v_r\rangle$ (by a factor of $\sim$2) absent CRs. Outflow rates are similar near the disc ($r\lesssim30$ kpc): runs without CRs actually have larger $\dot{M}_{\rm out}$, with $\sim2-3\times$ 'faster' mean $\langle v_r\rangle$ ($\gtrsim100$ km s^{-1}). But in the CGM ($\gtrsim30$ kpc), absent CRs the outflow is dramatically 'halted,' while with CRs it actually accelerates and $\dot{M}_{\rm out}$ increases again, to give $\dot{M}_{\rm out}>\dot{M}_{\rm in}$ at essentially all radii $\gtrsim100$ kpc. The CR outflows have intermediate $|\langle v_r\rangle^{\rm out}|\sim|\langle v_r\rangle^{\rm in}|\sim50-100$ km s^{-1}. Without or without CRs, outflow metallicities decrease with r, indicating continuing entrainment, but with CRs the trend is monotonic at all r and the outflows have higher metallicity (versus inflow) at all r (while outflows absent CRs mix within $\sim R_{\rm vir}$, giving no inflow/outflow difference).

we see $\dot{M}_{\rm out}$ fall then rise to dominate over inflow $\dot{M}_{\rm in}$ over >Mpc scales, with a mean velocity which increases to $\sim$ 70–80 km s^{-1} out to $\sim$ 1.5–2 $R_{\rm vir}$.

Fig. 6 goes a step further and follows the time-history of Lagrangian gas elements in the CR+ simulation. The fast outflows at large-r are accelerated over a broad range of radii in good agreement with our simple analytical expectations for constant $\rho/\rho_{\rm crit}$, without necessarily being heated to (or spending much time at) 'hot' temperatures $T\gtrsim10^6$ K where cooling is inefficient. In fact, the outflows tend to begin 'cold' (at typical ISM temperatures $\sim10^4$ K) and are mildly photoheated as they expand (roughly tracing photoionization equilibrium with the UV background, with $T\propto\rho^{-0.2}$ or so; see Ji et al. 2020). For the kinematics, we specifically compare the predicted v_r of r obtained from the model in Section 3 if we take the actual $V_c(r)$ from the simulation and assume a fixed ratio $\rho\approx\rho_{\rm crit}/2$ (approximately what we see for the fast winds in Fig. 5), for material starting at $r\approx10$ kpc. This provides a remarkably good description of the fast outflows.

Fig. 5 shows the outflow velocities, densities, and temperatures at a *fixed* time in a specific radial annulus, to show that even at a fixed time, and at a given radius, the CR+ simulation outflow velocities trace our simple analytical expectation for the 'terminal' velocity at a given density given acceleration by the CR pressure gradient, while remaining at the relatively cool/warm temperatures given by photoionization equilibrium. In contrast, in the 'No CRs' runs, the outflows are strongly associated with gas whose thermal temperature exceeds the virial temperature, suggestive of traditional hydrodynamic pressure-driven outflows.

All of these behaviours are clear demonstrations of CR acceleration in the 'CR+' run. In fact, the acceleration we see in the CR+ runs is not generically possible for an energy *or* momentum-conserving hydrodynamic wind. Consider: over much of the range of spatial scales where we see the outflows, the gas follows a density profile of approximately $\rho\propto r^{-1}$ (which follows from $\rho\sim\rho_{\rm crit}\propto1/(r\,V_c^2)\sim1/r$ over the range where V_c ~constant, approximately $\sim$ 20–100 kpc here). In this regime, the velocities of a

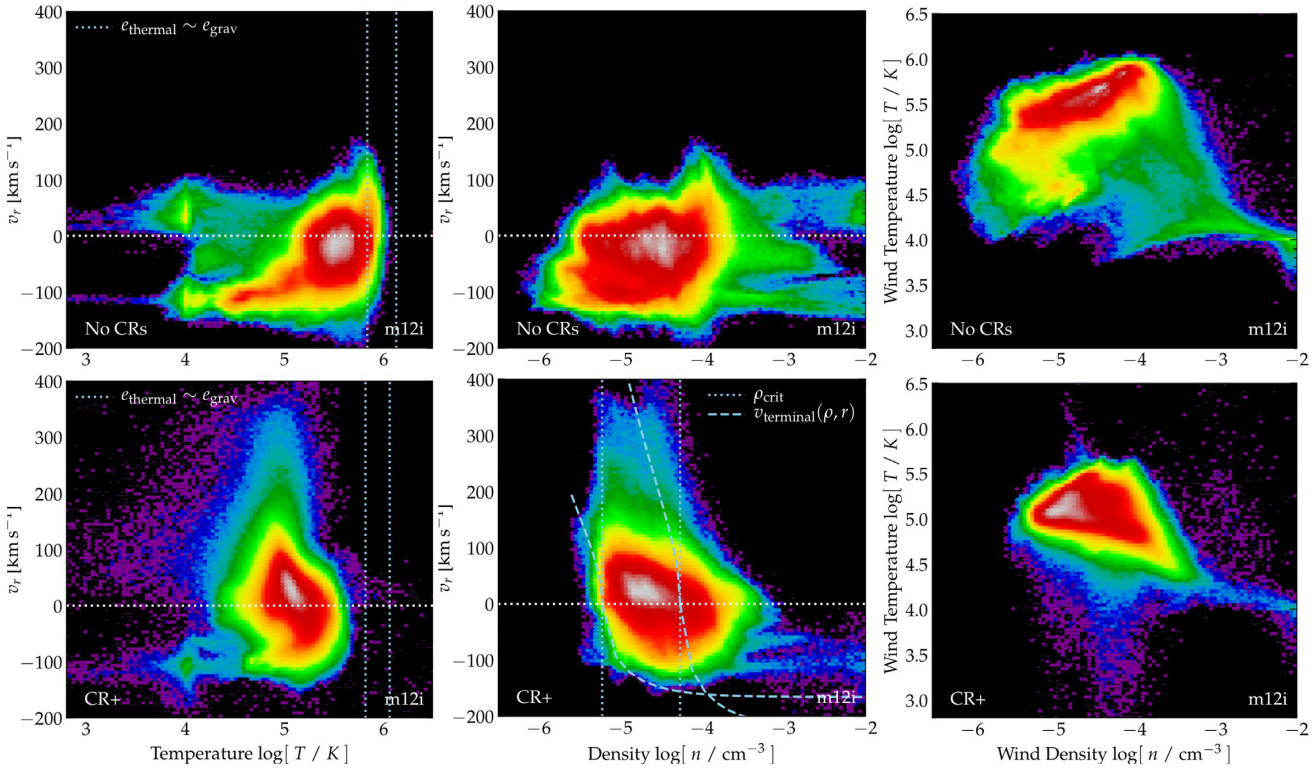

Figure 5. Distribution of gas outflow properties (as Fig. 1), comparing our default **m12i** 'No CRs' (*top*) and 'CR+' (*bottom*) runs. *Left:* Gas outflow velocity (v_r) versus temperature T, for gas selected at galactocentric radii $0.5 < r/R_{\rm vir} < 1.5$. Vertical lines show the value of T at the inner/outer radii in the 'slice' where the gas thermal energy density would equal the gravitational potential. In the 'No CRs' run fast outflows preferentially appear in 'hot' gas which nears this virial-like value. In the 'CR+' run, the outflows are 'cool' ($T \sim 10^5$ K, well below this virial value). *Middle:* Outflow v_r versus density n, in the same slice in r. Vertical dotted lines label $\rho_{\rm crit}$, the critical density (Section 3) where CR pressure balances gravity on the gas, at the inner/outer slice r. Dashed curves label the analytical expected 'terminal velocity' for gas which deviates from $\rho_{\rm crit}$ (denser gas falls in under gravity, less dense gas accelerates out under CR pressure; see Section 3). Without CRs, there is no density-v_r relation; with CRs, most gas resides near $\rho_{\rm crit}$, and lower density gas preferentially flows out while higher-density gas almost exclusively flows in. *Right:* Phase ($n - T$) diagram of outflow material (selected to have $v_r > V_{\rm vir}/2$): the 'CR+' outflows are cooler and lower-density, on average.

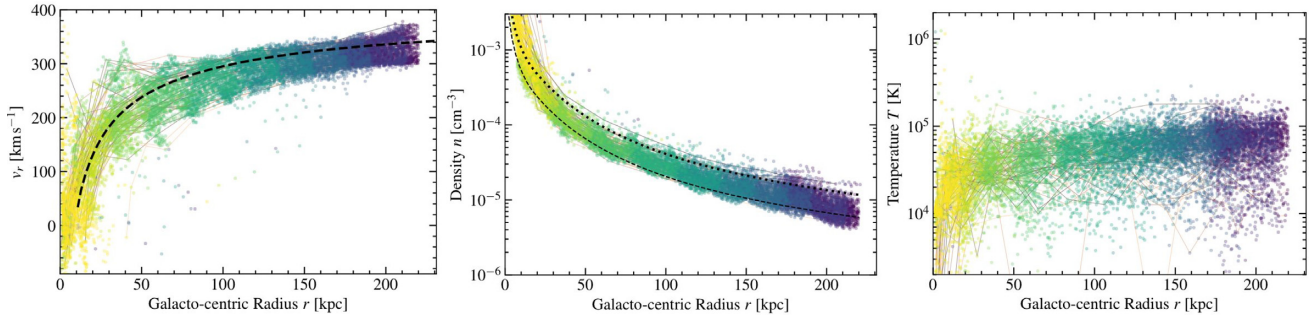

Figure 6. Time-evolution of the 'fast' outflows in the CR-dominated **m12i** halo (Fig. 1; 'CR+'). To define this, we select all gas with $175 < r/{\rm kpc} < 220$ and $300 < v_r/{\rm km\,s^{-1}} < 400$ at $z = 0$, and follow the Lagrangian histories of those fluid elements back to redshift $z \approx 0.07$ (~ 1 Gyr lookback time). Points show different Lagrangian fluid elements at each snapshot in time, with colours/brightness indicating increasing lookback time (black-to-yellow, in ~ 50 Myr increments); for illustrative purposes, we select a random $\sim$50 elements and show lines connecting their trajectories. Note this is only the selected 'fast' component – not the average of all gas (which is much slower) shown in Fig. 4. *Left:* Radial velocity and galactocentric r, as a function of time. Thick (dashed) line shows the analytical prediction from Section 3 (as Fig. 5) for a CR pressure-accelerated outflow originating at ~ 10 kpc with $\rho \sim (2/3)\,\rho_{\rm crit}$. *Middle:* Density and r versus time. Dotted line shows the equilibrium $\rho_{\rm crit}$ (Fig. 5), dashed line shows (1/2) of this: the outflow 'launches' where the gas falls below $\rho_{\rm crit}$ and is accelerated continuously while just modestly below this density at each r. *Right:* Temperature and r versus time. The outflows 'begin' cold in the disc, and are never heated to sustained very high temperatures before or during acceleration.

hydrodynamic wind with constant energy input ($\dot{E}_{\rm wind}$) or momentum input ($\dot{P}_{\rm wind}$) rates, or a conserved/constant initial/impulsive energy or momentum ($E_{\rm wind}$ or $P_{\rm wind}$) would necessarily decrease with r (following a given fluid element).

4.1.2 *Outflow phases and metallicities*

As noted above, in the CR+ run, the outflows lie preferentially at somewhat lower densities (as this material is efficiently accelerated outward by CR pressure gradients) and lower temperatures (as the

acceleration is non-thermal and the densities low, most of this gas is simply at the equilibrium temperature for photoionization by the UV background), compare to our non-CR simulations. This is part of a broader trend examined in detail in Ji et al. (2020), wherein the *entire* CGM (both inflow and outflow) is shifted in density and (more dramatically) temperature when the halo is dominated by CR pressure (so gas can remain in the halo at thermal pressures well below virial).

We also see in Fig. 6 that the 'slow' outflows at larger radii contain a mix of some decelerated fast material, but also material which is accelerated *in situ* at large $r \gtrsim R_{\rm vir}$ – material which *never* enters the galaxy. This also means that the metallicity of the outflows does not necessarily trace that of the galaxy, depending on where the material is 'swept up.' We see this in Fig. 4, where the metallicity of the outflows steadily decreases with galactocentric distance, clearly indicating 'new' (lower-metallicity material which was residing in the halo) gas is swept up (either directly entrained or accelerated *in situ*) to join this outflow. This occurs to some extent as well in our non-CR runs (and is discussed in detail in Muratov et al. 2015 and Ma et al. 2016), but the trend is much more clear and monotonic in the CR runs. This has a very important consequence: depending on where one defines or measures the outflow, it's metallicity can be much lower than the ISM metallicity (which is roughly the wind metallicity at the base of the disc), and so its 'metal-loading' factor can be much lower than its mass-loading factor.

4.1.3 *Outflow geometry and morphology*

Figs 2and 3 clearly illustrate a dramatic change in the morphology and geometry of inflows and outflows between our No CRs and CR+ runs. Absent CRs, the gas forms a quasi-spherical virial shock (at a radius of $\approx 1\ R_{\rm vir}$). External to the virial shock, the gas is in spherical inflow, while internal, it is largely turbulent, with outflows from the galaxy 'stalling' and driving strong mixing with the CGM gas as they recycle. With CRs, the virial shock is hardly evident (the actual changes to the virial shock structure will be studied in future work), and the outflow and inflow assume a clear biconical structure which is also bipolar (approximately aligned with the angular momentum vector of the galactic disc). Inflow proceeds in the dense mid-plane sheets and filaments and joins smoothly on to the rotating disc at ~ 20 kpc. Outflow extends outwards biconically with a widening outflow angle at increasing distance, filling the majority of the volume of the CGM and IGM out to $\sim$ Mpc distances.

Note that the alignment of the outflows and the inner (~ 10 kpc) disc axis is not perfect in Fig. 3. Moreover, we show below some example galaxies where the bipolar outflow 'base' is well above the disc (at $\sim$ 30–50 kpc above the disc) as opposed to joining on to the disc. We also find that the disc orientation can sometimes vary (owing to e.g. minor mergers) on relatively short ($\lesssim$Gyr) time-scales, but the outflow geometry on large scales remains stable. We also argued above that much of the outflow is accelerated well above the disc in the CGM. And we see the outflow is not particularly biconical, even very close to the disc, in our 'No CRs' runs. All of this strongly argues that the bipolar morphology of the CR-driven outflows is *not* a result of 'shaping' by the disc (as occurs for e.g. nuclear pressure-driven outflows emerging from a disc). Rather, the direction and morphology of *both* the outflows and the disc follow from a common cause – the geometry of the large-scale IGM accreting on to the halo. The dense planar/filamentary structures accreting on to the halo define the preferred angular momentum axis and hence, disc direction, but they also define the directions where CR pressure will not overcome inflow ram pressure. Instead CR pressure will drive outflows in the remaining, lower-density volume that has lower ram pressure.

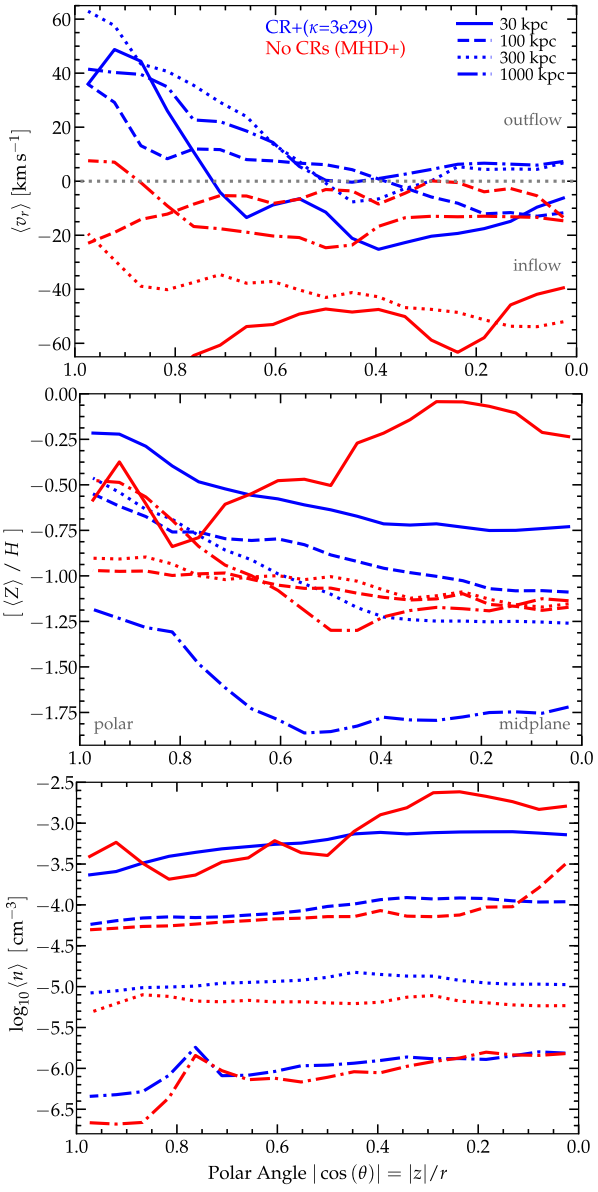

Figure 7. CGM gas properties versus polar angle $\cos\theta = z/r$, where $\hat{z}$ is the direction of the disc angular momentum axis within 10 kpc, in four spherical shells at radii $r = 30,\ 100,\ 300,\ 1000$ kpc. We compare mass-weighted mean gas radial velocity ($\langle v_r \rangle$; *top*), metallicity ([Z/H]; *middle*), and density ($\langle n \rangle$; *bottom*), in runs with (*blue*) and without (*red*) CRs. Mean densities are similar with or without CRs: $\langle n \rangle$ decreases primarily with r (as $\sim r^{-2}$, roughly), with a weaker trend with θ (polar $\langle \rho \rangle$ a factor of $\sim$3 lower than mid-plane). Absent CRs, there is little coherent trend in Z, with CRs a monotonic radial trend is evident with again a weaker θ-dependence (factor of $\sim$3 higher Z at poles). In $\langle v_r \rangle$, we see a clear trend with CRs where polar angles are in outflow (accelerating away from the disc) with mid-plane inflow (accelerating near the disc); without CRs there is no polar-angle trend.

Fig. 7 quantifies the angular dependence of outflow/CGM properties in more detail. We see that the mean density profile of the CGM is relatively weakly modified by CRs. This is consistent with the conclusions in Ji et al. (2020), who showed the effects on CGM temperatures were much larger. There is a strong radial density

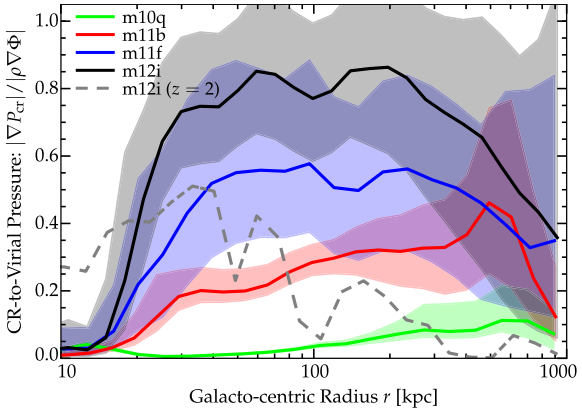

Figure 8. Ratio of the outward CR pressure force $\nabla P_{\rm cr}$ (averaged in spherical shells at a given radius r) to gravitational force $\rho\,\nabla\Phi$ at the same r, as a function of r (solid line shows mean; shaded shows inter-quartile range), at $z = 0$ (except for one line measured at $z = 2$, labelled), for different haloes from Table 1. As shown in Paper I and Ji et al. (2020), in the simulations with CRs (with these particular diffusion coefficients), CRs dominate the CGM pressure for MW-mass galaxies at low redshifts $z \lesssim 1$. At lower masses (or higher redshifts), the CR pressure (relative to gravity) drops rapidly, becoming negligible for galaxies with haloes $\lesssim 10^{11}\,{\rm M}_\odot$ (or $z \gtrsim 1$–2). At $\lesssim 20$ kpc, we see the effect of the gaseous disc (where rotation, not hydrostatic CR pressure, balances gravity); at $\gtrsim 200$ kpc, we see mean CR pressure falls but some sightlines with low densities still have $|\nabla P_{\rm cr}| \sim |\rho\,\nabla\Phi|$, so slow CR-pressure-driven outflows can continue to ∼Mpc.

gradient (as expected), and a weaker trend at all radii towards lower density in the poles – this occurs even outside $R_{\rm vir}$ in the 'No CRs' runs, indicating it follows from large-scale structure. With CRs, there is a more well-ordered metallicity trend (discussed above), with higher metallicity in the polar direction (owing to outflow). Together these offsetting effects mean that the metal columns are not wildly different in the polar and planar directions. The velocity, as expected from Figs 2 and 3, shows the most clear difference between no-CR and CR+ runs, shifting from essentially no angular dependence at any radius in 'No CRs' to clearly polar structure in 'CR+.'

4.2 Scaling with halo mass and redshift

Having considered a detailed case study of one galaxy (**m12i**) above, we now use our larger sample of simulations to explore how the effects of CR-driven winds scale as a function of galaxy mass. Recall, Paper I showed that the effects of CRs (from SNe) on galaxy properties dropped off steeply at halo masses $M_{\rm halo} \lesssim 10^{11}\,{\rm M}_\odot$ or redshifts $z \gtrsim 2$. Ji et al. (2020) showed the same for the effects of CRs on CGM phase structure. This is also naturally predicted by the simple analytical scalings in Section 3: at low $M_{\rm halo}$, the ratio $M_*/M_{\rm halo} \propto \dot{M}_*/M_{\rm halo} \propto \dot{E}_{\rm cr}/M_{\rm halo}$ drops precipitously – there simply isn't enough energy in CRs to compete with other forces (moreover, mechanical input from SNe becomes more efficient, further limiting the relative contribution of CRs). And at high-z, high densities within the galaxy deplete CR energy collisionally while dense haloes contribute greater pressure than CRs can support.

Fig. 8 illustrates this showing the CGM pressure support from CRs, now comparing some $\sim 10^{10}$, 10^{11}, and $10^{12}\,{\rm M}_\odot$ haloes. We see that by $< 10^{11}\,{\rm M}_\odot$, CR pressure is not sufficient to provide hydrostatic equilibrium support (we show in Paper I that at all radii in these haloes, the gas thermal pressure is larger than the CR pressure). By $\sim 10^{10}\,{\rm M}_\odot$, the CR pressure is more than an order-of-magnitude sub-dominant at all radii. We therefore expect the effects seen in **m12i** ($\sim 10^{12}\,{\rm M}_\odot$) to drop off rapidly in our less massive haloes below $\sim 10^{11}\,{\rm M}_\odot$. Fig. 9 shows the inflow/outflow rates of gas and SFRs at several haloes across this mass range: indeed, the effects on galaxy SFRs (as shown in detail in Paper I) drop off rapidly and become second-order or negligible below $M_{\rm halo} \lesssim 10^{11}\,{\rm M}_\odot$, and we see the same in the outflow rates and velocities at any radii. By the lowest-mass ($10^{10}\,{\rm M}_\odot$) haloes the outflows become strongly dominated by the effects of the most recent large 'burst' of SF.

Figs 10, 11, and 12 repeat our study of the outflow/inflow velocity distribution versus radius, density, and temperature. For the haloes with $M_{\rm halo} \gtrsim 10^{11}\,{\rm M}_\odot$, we find in every case qualitatively similar conclusions to our **m12i** case study, with the effects generally becoming stronger in the more massive haloes, as predicted, while they drop off at lower-mass haloes. A couple of the 'marginal' cases are interesting: the effects of CRs on the CGM and outflows of e.g. **m11q** are stronger here than they are on its stellar mass and CGM properties (see Paper I), but this halo lies exactly at $\sim 10^{11}\,{\rm M}_\odot$ (the border between weak/strong CR effects), so this is perhaps not surprising. Where the CR pressure is weak (in lower-mass haloes), we see our analytical prediction for the CR-pressure driven outflow velocities falls well short of the actual velocities: this is just the statement that the outflows are not CR-driven.

Closely related, Fig. 13 shows the outflow velocity distributions in the CGM and CGM + ISM of the galaxies. Again at low masses, there is no significant difference. At high masses, this quantifies again the extent to which ISM outflows are pressure-confined in the massive haloes without CRs, while high-velocity material primarily resides at large radii in the CR-dominated haloes.

Figs 14, 15 and 16 (see also Figs. A1, A2, A3, A4 in the Appendix) repeat the morphological comparison of inflows and outflows on CGM/IGM scales. Again in more massive haloes, the qualitative conclusions match **m12i**. The radii and mass range where the outflow/inflow morphology is strongly altered corresponds to those where CRs strongly alter the total pressure balance, in Fig. 8. In low-mass haloes, the morphology is dominated by the shocks from outflowing gas, and turbulence, but is not particularly sensitive to the presence of CRs.

Note that in many of these plots, in the low-mass systems (e.g. **m10q**, **m10v**) we can clearly see in both the CR+ and non-CR runs, the impact of successive 'bursts' of SF on the CGM/IGM: they produce successive 'spikes' of outflowing material ('shells' with $v_r \propto r$ over a small range, consistent with a burst of material launched at the same time), and a series of concentric shocks visible in the inflow/outflow morphology.

Fig. 8 also shows the effects of changing redshift. Again in Paper I, we showed in detail that the effects of CR pressure in the CGM decrease with increasing z (at fixed $M_{\rm halo}$ or M_*), even more rapidly than the effects drop off with lower halo mass – by $z \gtrsim 1$–2 (depending on the halo mass) the effects of CRs are completely negligible in the CGM pressure. We confirm this here. As a result, the effects of CRs 'shaping' the outflows are weak at high redshift, and we cannot identify any obvious morphological or quantitative differences at $z \gtrsim 2$ (but because high-redshift galaxies are quite 'bursty' and often undergoing mergers, side-by-side morphological comparisons such as those above tend to be dominated by chaotic differences in timing of bursts, etc.). So we do not explore this further here.

It is worth noting, as discussed further in Paper I, that some previous studies (e.g. Booth et al. 2013; Simpson et al. 2016) found stronger effects of CRs in dwarfs than we see here; however, that particular study included very weak mechanical feedback from SNe

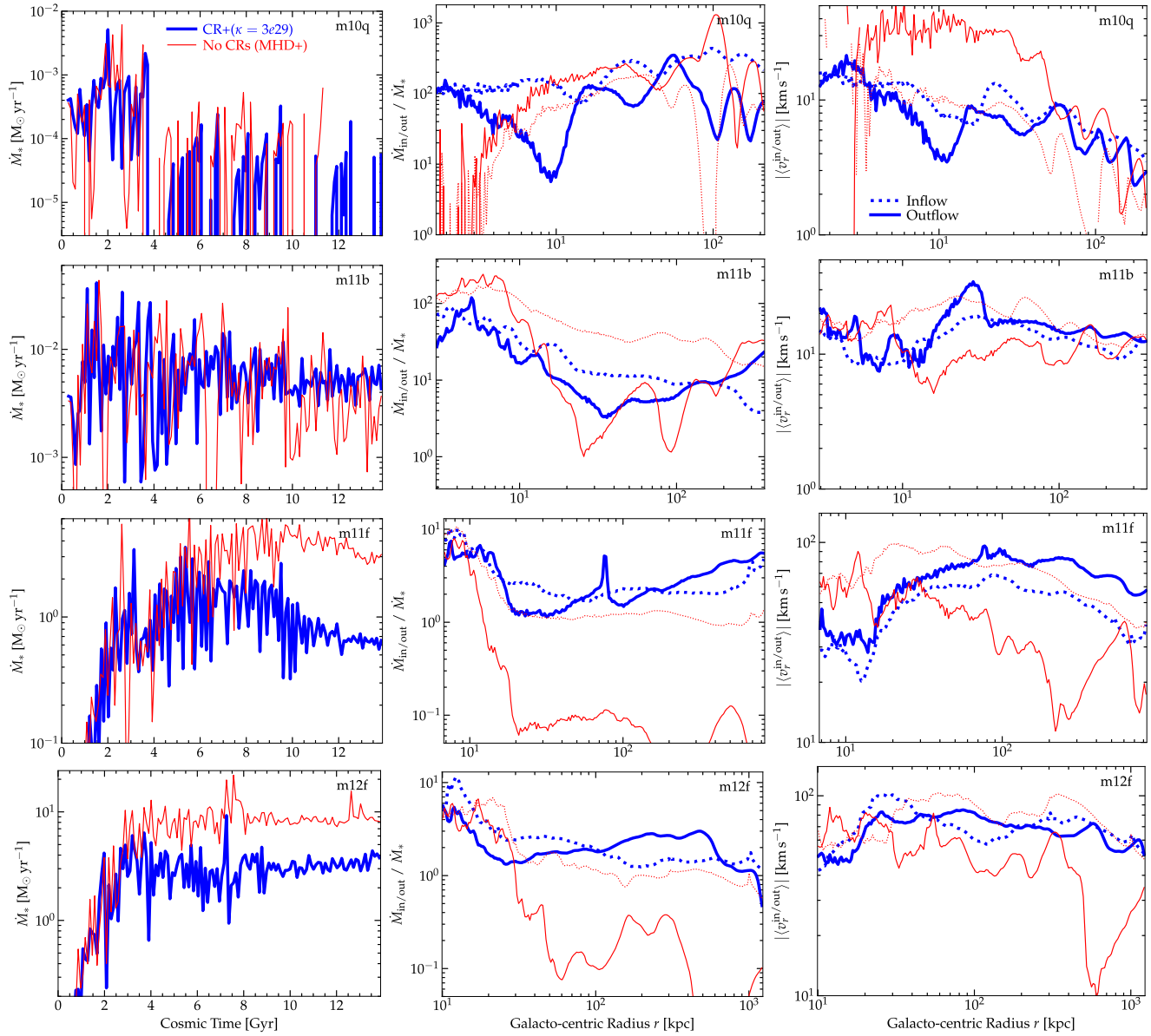

Figure 9. SFRs and inflow/outflow rates (as Fig. 4) for **m10q**, **m11b**, **m11f**, **m12f** (top-to-bottom; see Table 1). As expected from where CRs dominate the pressure in the halo, the CRs have a weak effect on the SFR (see Paper I) or mass outflow rate at any annulus in runs with $M_{\rm halo} \lesssim 10^{11}\,{\rm M}_{\odot}$ (**m10q** and **m11b**, here). There are some more subtle effects at these halo masses: note e.g. the somewhat less-bursty late-time SFR in **m11b** (which is reflected in the outflow rate having less pronounced 'peaks' at large r from those previous 'bursts'). But in haloes which reach $\gtrsim 10^{11}\,{\rm M}_{\odot}$ at $z\sim 1$ (**m11f**) or $z\sim 2$ (**m12f**), the effects are similar to those for **m12i** in Fig. 4: inflow rates at large radii, and outflow mass-loading factors at small radii ('near the disc') are relatively weakly modified, but CRs strongly suppress SF by accelerating material into outflow away from the disc in the CGM and IGM, maintaining net outflow with $\dot{M}_{\rm out}$ flat or rising to $\gtrsim$ Mpc.

(using a 'pure thermal energy deposition' scheme that the authors noted tends to over-cool), and a lower diffusivity by a factor of $\sim$100. Thus, CRs are more strongly trapped in the ISM (see Paper I), and SNe are relatively weak, so the relative effect of CRs is more prominent. As per Paper I, with higher diffusivity CRs escape dwarfs more efficiently (as observed; see e.g. Lopez et al. 2018), but more importantly with more careful coupling of mechanical SNe feedback and better resolution of superbubble cooling radii (see Hopkins et al. 2018b), the SNe mechanical energy (which is an order-of-magnitude larger than CR injection energy, by definition) simply dominates in dwarfs where cooling is often inefficient.

5 DISCUSSION AND CONCLUSIONS

We study the properties of galactic outflows in a large survey of high-resolution cosmological FIRE-2 simulations, with explicit treatment of mechanical and radiative stellar feedback (SNe Types Ia and II, O/B and AGB mass-loss, photoionization and photoelectric heating and radiation pressure), magnetic fields, anisotropic conduction and viscosity, and CRs injected by SNe (with anisotropic streaming and diffusion; advection and adiabatic interactions; hadronic, Coulomb and streaming losses). Previous work has extensively explored how mechanical and radiative feedback influence outflows, and has also

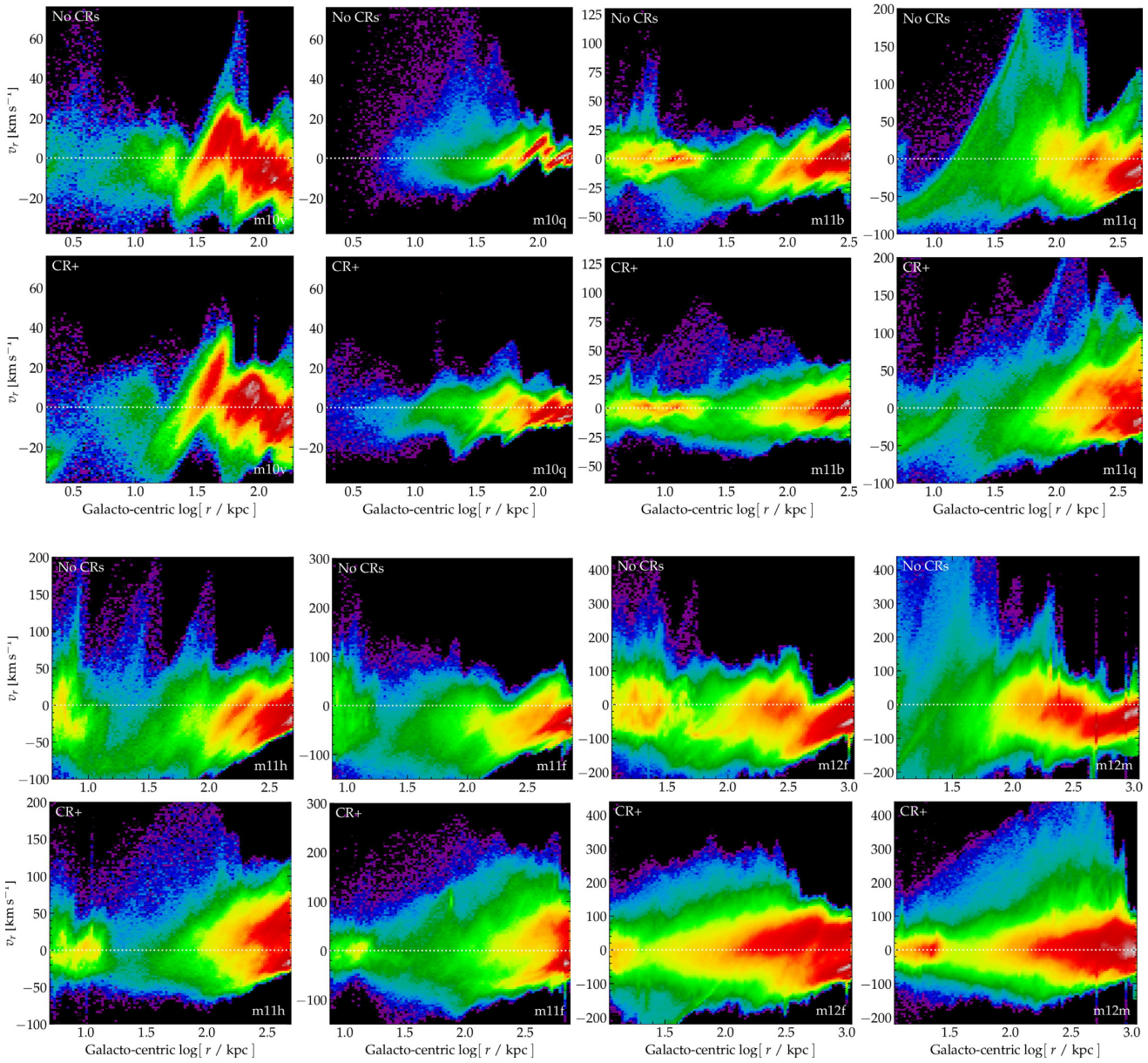

Figure 10. Gas outflow velocity versus radius, as Fig. 1, for a representative sub-sample of our simulated haloes ordered by mass (increasing left-to-right, in the top and bottom 'groups'), in our 'No CRs' (*top*) and 'CR+' (*bottom*) runs. Below $M_{\rm halo} \lesssim 10^{11}$ M$_\odot$ (top 'group'), the CRs have little obvious effect, consistent with their weak pressure relative to thermal (Fig. 8). At higher masses (bottom 'group') the features in Fig. 1 become progressively more prominent.

shown that their properties (at least in so far as relevant for bulk galaxy/ISM/CGM/IGM predictions) are not particularly sensitive to magnetic fields, conduction, and viscosity. We therefore focus on the role of CRs.

5.1 Key conclusions

In previous studies (see Paper I), we have shown that the effect of CRs (from SNe) on galaxy properties is maximized in intermediate and massive ($M_{\rm halo} \sim 10^{11-12}$ M$_\odot$) haloes at relatively low redshifts $z \lesssim$ 1–2. This is where, for physically reasonable and observationally allowed CR parameters (from γ-ray, grammage, CR energy density, synchrotron, and other constraints; see Paper II), CR pressure can dominate over gas thermal pressure in the halo. Not surprisingly, we find the same for outflows. Specifically, the effects of CRs on outflows are strongly correlated with their relative prominence in the CGM (e.g. ratio of CR to thermal gas pressure, at $\sim$ 0.1–2 $R_{\rm vir}$). Where this ratio is large, CRs dramatically alter outflows; where the ratio is small, they have small effects.

In 'CR-dominated' haloes (near this 'sweet spot' in mass and redshift, where CRs dominate the CGM pressure), we find the following effects on outflows and inflows:

(i) The morphology of outflows and inflows is drastically reshaped. In CR-dominated haloes, outflows are coherently biconical from disc-through-IGM ($\gtrsim$ Mpc) scales, with most of the *volume* at large radii in outflow, and inflow confined to relatively small covering-angle, dense planar/filamentary structures (Trapp et al., in preparation). Some collimation occurs even when CRs do not fully dominate, if they still contribute an order-unity fraction of the CGM pressure. Absent CRs, the biconical morphology is largely destroyed

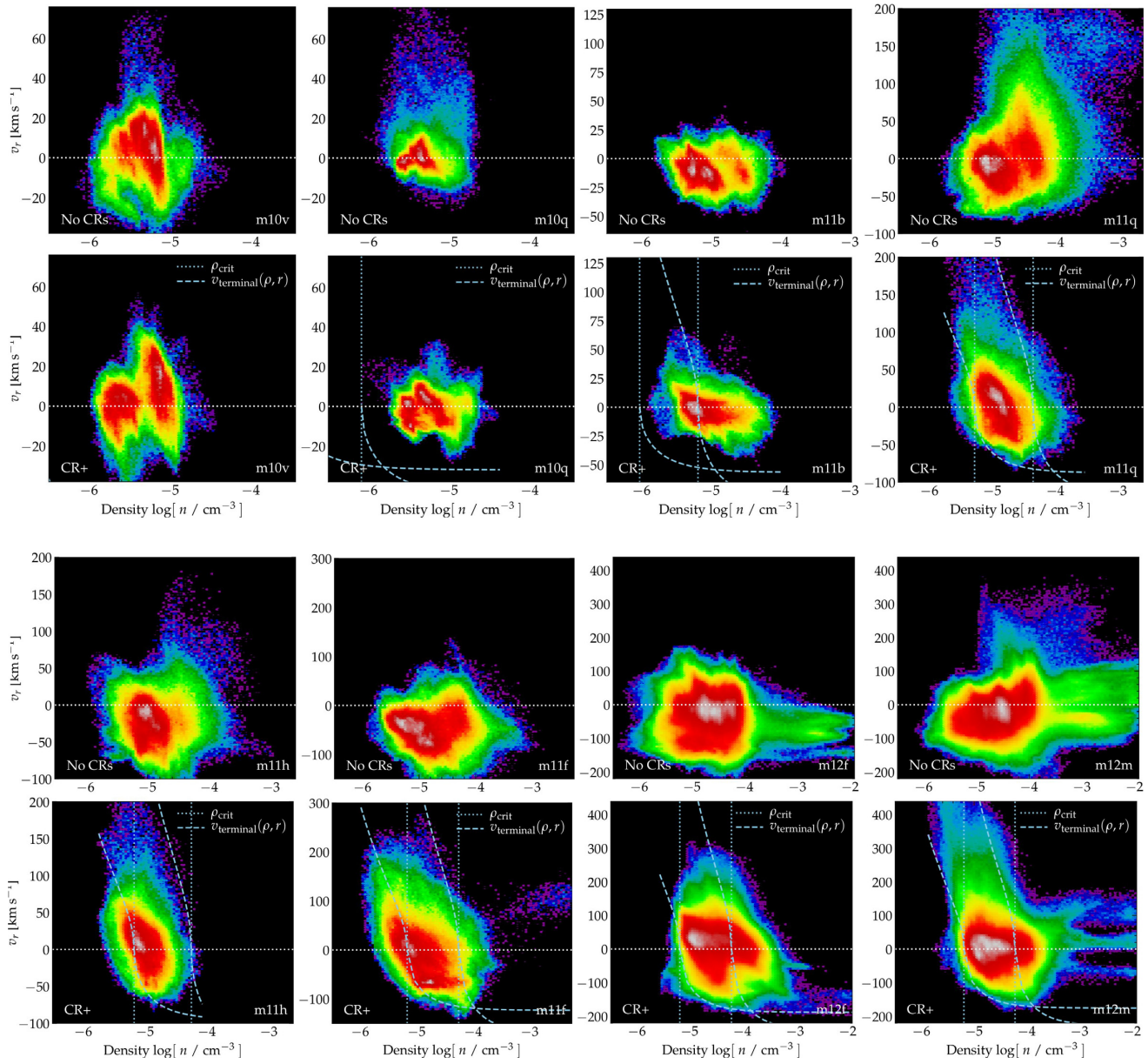

Figure 11. Gas outflow velocity versus density (as Fig. 5), for a sub-sample of our simulated haloes ordered by mass (as Fig. 10), in 'No CRs' versus 'CR+' runs. For each, we select gas with $0.5 < r/R_{\rm vir} < 1.5$, and compare the equilibrium $\rho_{\rm crit}$ where CR pressure balances gravity, and $v_{\rm terminal}$ for acceleration by CRs + gravity (see Section 3 and Fig. 5). In low-mass ($\lesssim 10^{11}$ M$_\odot$) haloes, $\rho_{\rm crit} \ll \rho$ and $v_{\rm terminal} \ll v_r$, which simply reflects the fact that CRs make up a negligible contribution to the pressure (Fig. 8). Above this mass, the simple analytical scalings work remarkably well.

and what little outflow remains in $\sim L_*$ haloes is confined to the near-region around the disc, and essentially all directions show inflow on to the halo outside $R_{\rm vir}$.

(ii) The total or gross cosmological inflow rates on to haloes (at large radii) are not dramatically altered, although inflows appear to be slower (more 'gently' decelerated as they enter the CGM and approach the galaxy) and the virial shock is much less pronounced (this will be studied in future work; Ji et al. 2020). However, in CR-dominated haloes, the inflow is primarily confined to dense inflow structures (e.g. filaments) that carry most of the mass (primarily in the plane of the disc), but represent little volume or covering factor. Absent CRs, nearly all gas outside $R_{\rm vir}$ is inflowing.

(iii) Outflow rates *within and near the disc* ($r \lesssim 30$ kpc, in MW-mass systems) both absolute and per-unit-SF, are comparable or larger *without* CRs, and the mean velocities and temperatures of outflowing material are also larger ($v_r \gtrsim V_c$, and $k\,T \gtrsim \mu\,V_c^2$) without CRs. However, in massive haloes absent CRs, this outflow is strongly confined by the very large thermal gas pressure of the overlying halo, and so outflows decelerate and 'halt' rapidly outside the galaxy (recycling quickly and stirring the central regions; see Muratov et al. 2015, 2017). Where CRs dominate the pressure, outflows from the centre can escape, owing to the much lower thermal gas pressure of the halo (owing to rapid diffusion, the CR pressure does not 'resist' outflow expansion), and propagate effectively to extremely large radii $\gtrsim$ Mpc.

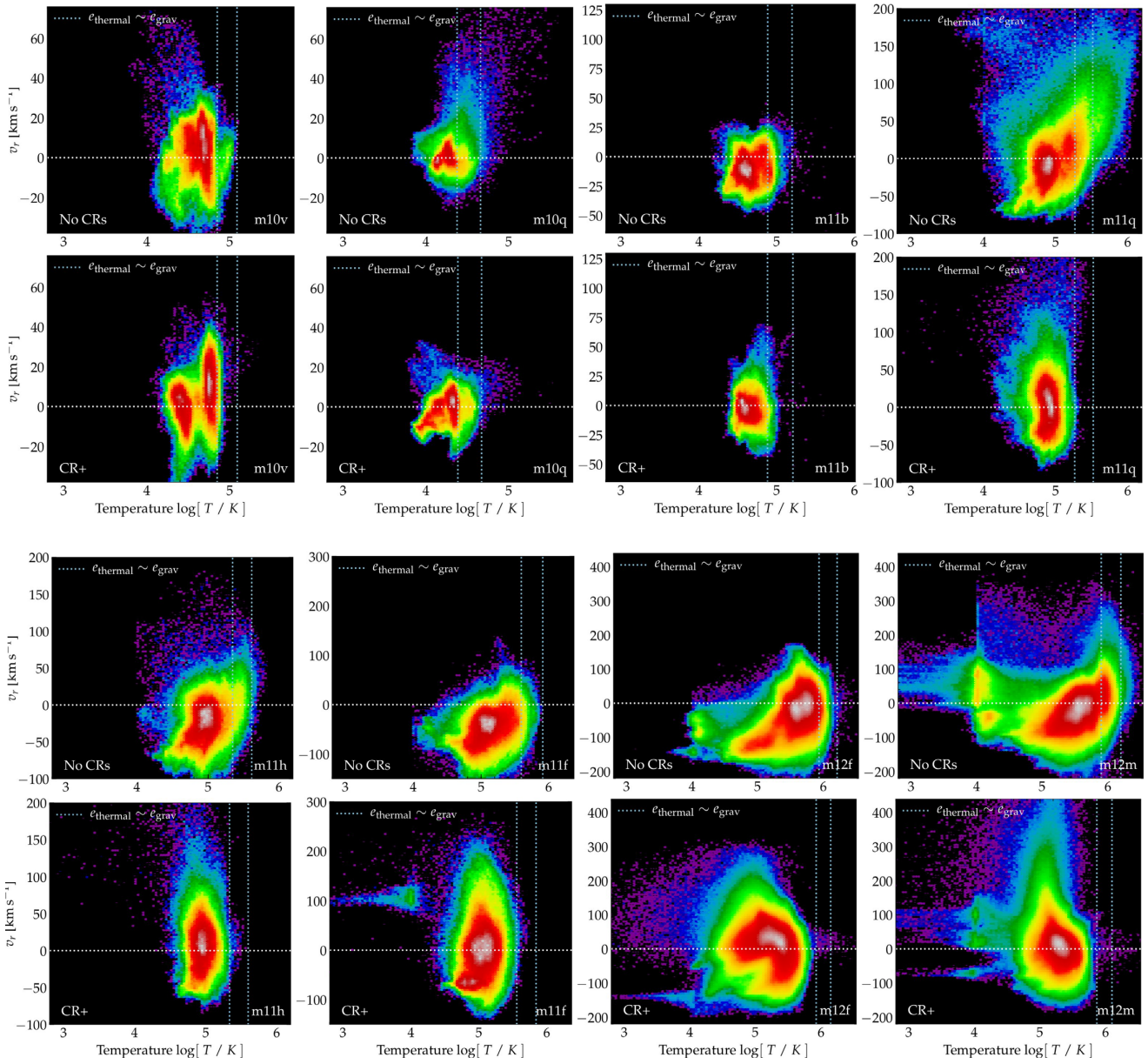

Figure 12. Gas outflow velocity versus temperature (as Fig. 5), for haloes ordered by mass in 'No CRs' versus 'CR+' runs (as Fig. 11, in the same r 'slice'). There is little difference in low-mass haloes but in high-mass haloes, outflows in 'No CRs' runs are preferentially 'hot' gas ($e_{\rm thermal} \sim e_{\rm grav}$), while in 'CR+' runs the outflows are primarily 'cool' ($T \sim 10^{4-5}$ K).

(iv) In CR-dominated regimes, gas is also accelerated '*in situ*' in the halo to large velocities by the large-scale CR pressure gradient (on $\sim$ 10–10^3 kpc scales). There is a critical density $\rho_{\rm crit}$ in the CGM, as shown in Paper I and Ji et al. (2020), where CR pressure balances gravity; less dense material is accelerated rapidly to $v_r \sim V_c(r)$ by CR pressure gradients. We show this '*in situ*' acceleration provides a good explanation of the wind dynamics, both for (i) material escaping the central $\sim$ 10–30 kpc and reaching large radii as 'fast' outflows (because V_c where it is accelerated is large), and also (ii) for accreted material which never reaches the galaxy and is 'turned around' or accelerated '*in situ*' at large $r \gtrsim R_{\rm vir}$ into 'slow' outflows ($v_r \lesssim V_{\rm vir}$).

(v) These effects (in the CR-dominated regime) directly supply CR-driven outflows at large radii, so the outflow rate or mass-loading actually *increases* further away from the disc, reaching and sustaining *net* outflow (compared to cosmological accretion rates) at essentially all radii $\gtrsim$ 100 kpc. Thus, CRs act primarily as a 'preventive' feedback mechanism: they suppress inflow rates into the galaxy and inner CGM, and extend the recycling times of gas that has already been blown out of a galaxy.

(vi) The less-efficient 'trapping' in CR-dominated cases means that outflows are not recycled nearly as rapidly as they are in runs without CRs. It is therefore important to revisit previous calculations based on following fluid elements over time, which argued that galactic outflows may be recycled many times at low redshifts in the CGM of massive galaxies.

(vii) Because the acceleration by CRs does not depend (directly) on gas thermal energy, and more so because much of the material

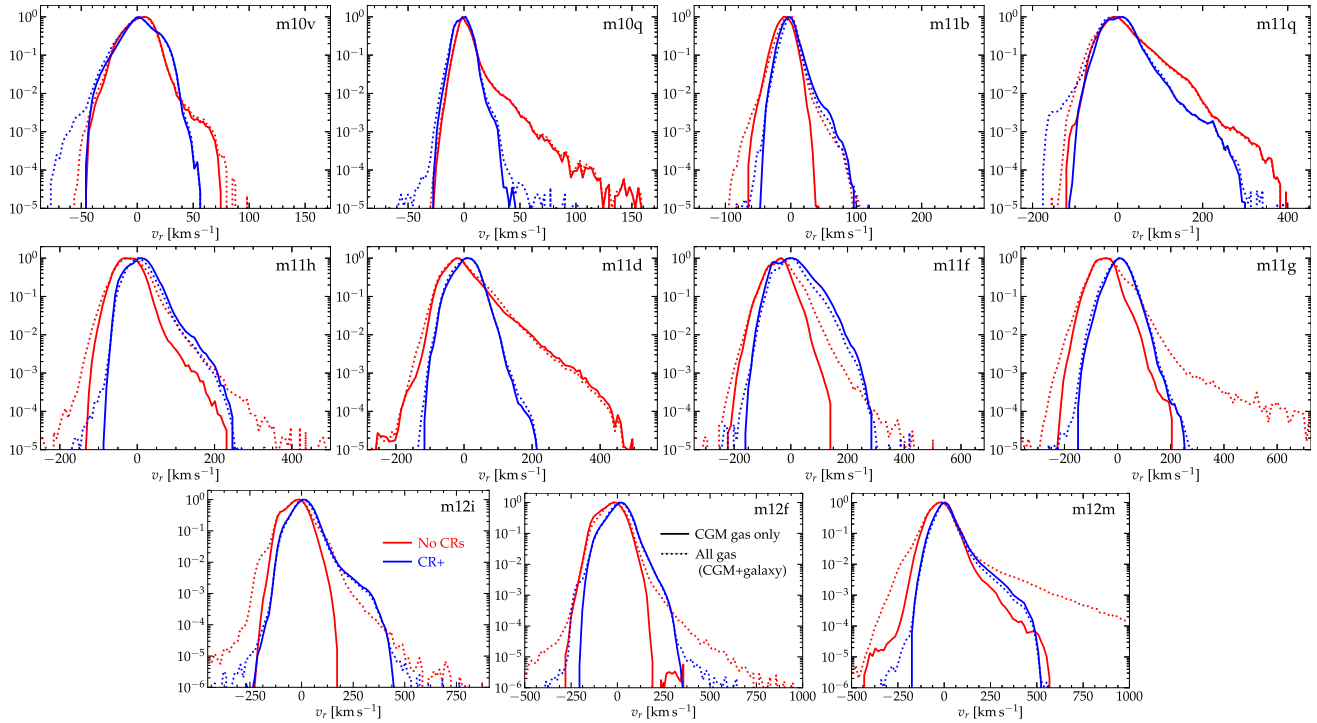

Figure 13. Radial velocity (v_r) distribution of gas in several simulations, ordered by mass. We compare the mass-weighted distribution of dP_M/dv_r of gas at $z = 0$ either (a) including all gas within $r < 1.5\,R_{\rm vir}$, or (b) including just CGM gas at $0.2\,R_{\rm vir} < r < 1.5\,R_{\rm vir}$. In our low-mass dwarfs (*top*; **m10v,q**, **m11b,q**), there are differences but these are dominated by stochastic fluctuations in 'bursty' SF and outflow. In both 'No CRs' and 'CR+' runs at low masses, the tail of higher-velocity material is similar whether we consider 'all gas' or 'CGM gas only,' indicating that outflows are not strongly 'trapped.' In more massive galaxies, the 'No CRs' runs commonly produce more high-velocity outflow when considering *all* gas, but this high-v_r tail is strongly suppressed when we restrict to CGM gas, indicating outflow trapping/stalling in the inner halo ($R < 0.2\,R_{\rm vir}$). As a result, the outflows *in the CGM* are stronger and reach higher velocities in the 'CR+' runs.

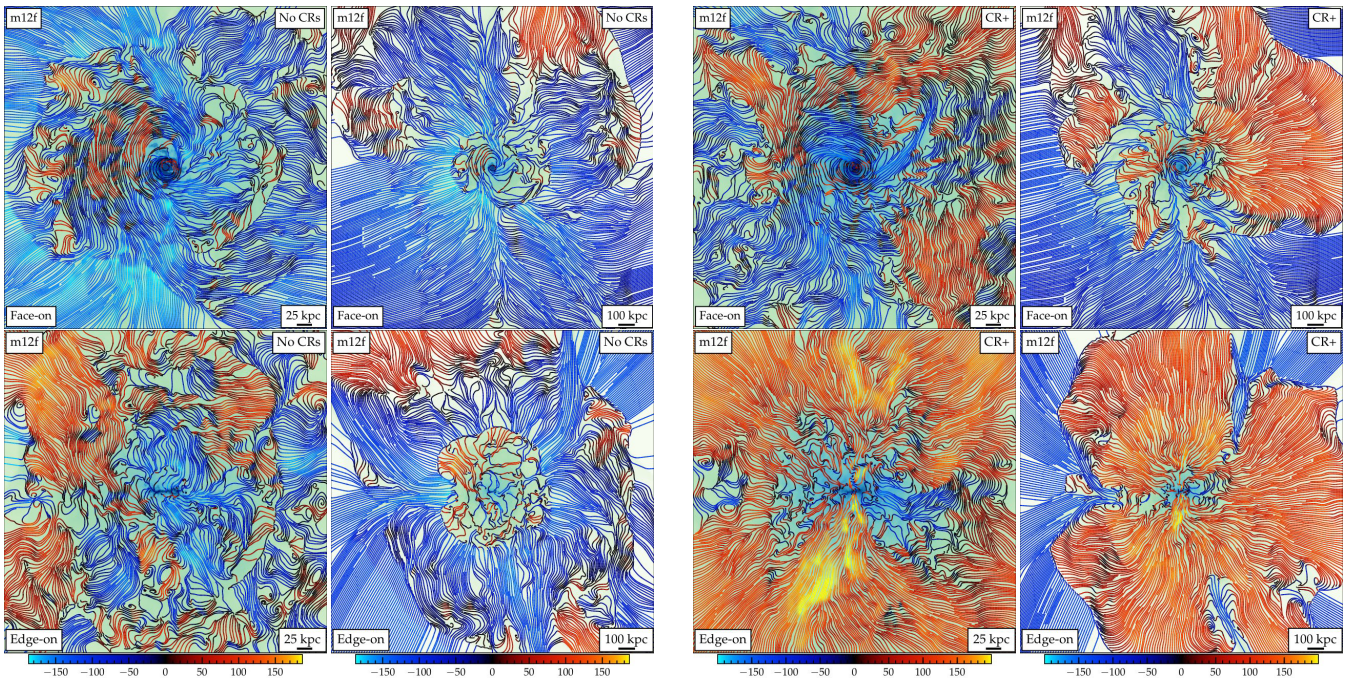

Figure 14. As Fig. 2, for halo **m12f**, comparing the 'No CRs' (*left* group) and 'CR+' (*right* group) runs, projected face-on (*top*) and edge-on (*bottom*) to the disc, at two different spatial scales (within $\pm R_{\rm vir}$, *left*, or $\pm 4\,R_{\rm vir}$, *right*). Colour bar gives v_r in km s^{-1}. Like **m12i**, the 'No CRs' run exhibits inflows from $\gg R_{\rm vir}$ scales and a sharp virial shock with a turbulent halo; while the 'CR+' run exhibits volume-filling outflows to >Mpc. These are broadly bipolar at $\sim R_{\rm vir}$ scales, but this becomes more volume-filling on larger scales with only narrow mid-plane channels continuing inflow.

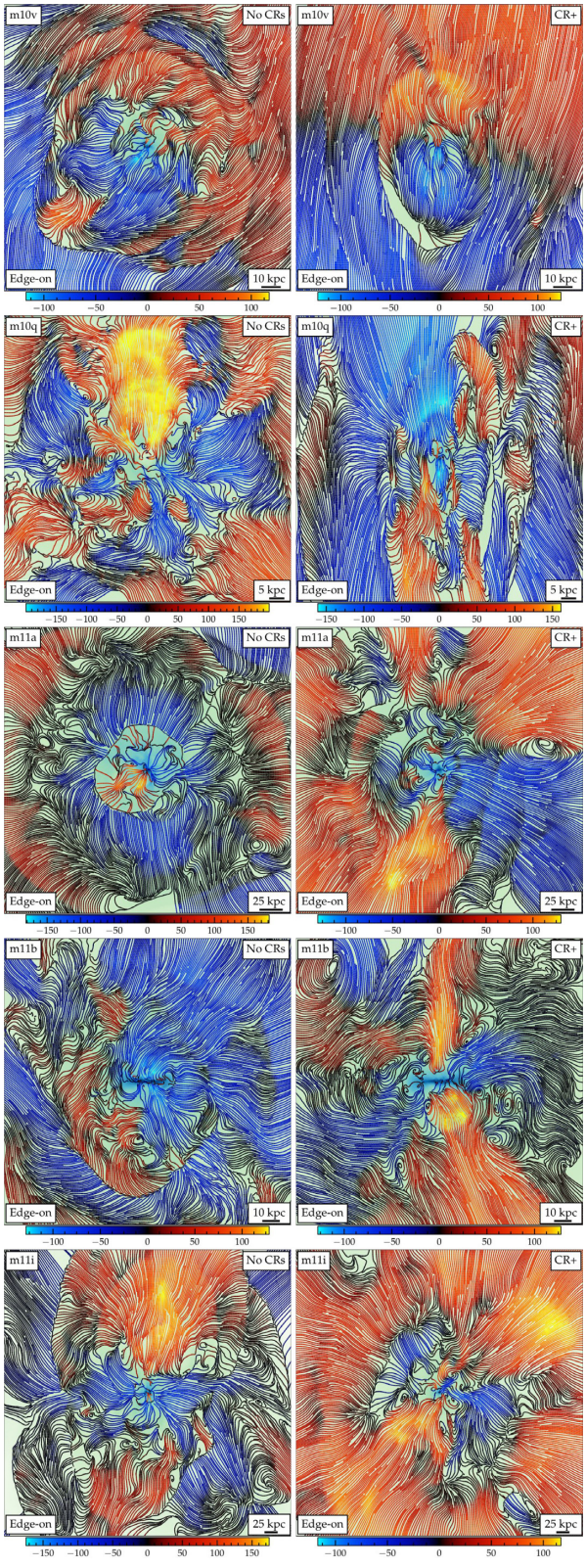

Figure 15. As Fig. 2, showing just edge-on projections, for 'No CRs' (*left*) and 'CR+' (*right*) runs of **m10v**, **m10q**, **m11a**, **m11b**, **m11i** (top-to-bottom, increasing mass). Spatial scale and v_r (in km s^{-1}). At the lowest masses, CRs have a weak effect (outflows can be stronger or more polar in 'No CRs' runs, depending on the recent SF history), while at higher masses, a clear shock appears in 'No CRs' runs where outflow meets accretion while the 'CR+' runs begin to develop large-scale bipolar outflow.

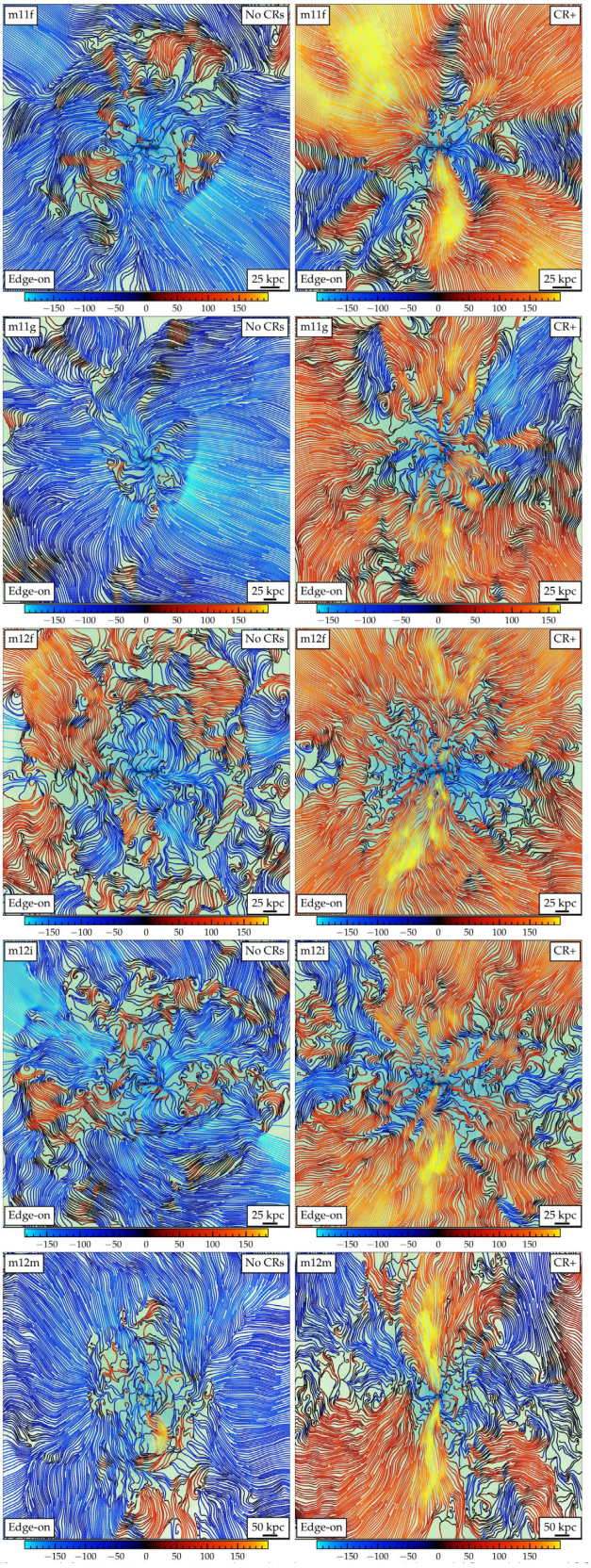

Figure 16. Fig. 15 continued to higher masses with **m11f**, **m11g**, **m12f**, **m12i**, **m12m**. The qualitative effect of CRs changing the CGM from turbulent quasi-spherical shock to coherent bipolar inflow-outflow, as in Fig. 2, is similar in each of these haloes.

at large radius is never shock-heated (even by the virial shock), the outflows in CR-dominated cases are primarily 'cool/warm' ($\sim 10^5$ K). This is a broader consequence, however, of the fact that the CGM as a whole is more dominated by gas which can be supported by CR pressure so does not need to have large temperatures to be in (initial) virial equilibrium (see Ji et al. 2020).

We show that all of the above phenomena can be predicted (with surprising accuracy) by simple equilibrium analytical scalings, derived in Section 3. These can also provide useful 'fitting functions' to predict CR pressure-driven outflow rates and velocities, where relevant.

Although there has been considerable study in the literature of CR-driven outflows (see references in Section 1), most of this has focused either (a) on driving in or very near the disc (e.g. around the CR scale height above the disc plane), or (b) around extremely massive haloes (e.g. clusters) where the CRs are likely sourced by AGN. Although some of our conclusions are similar (e.g. CRs can re-accelerate pressure-confined winds and enhance the fraction of 'cool' gas in the outflows), what is truly remarkable here is the enormous spatial scale over which the CRs have a dramatic effect. In fact, we find that almost all of the most dramatic effects only occur at radii $\gtrsim 30$ kpc, and extend to radii $\gtrsim$ Mpc. Obviously, exploring these far-field CGM/IGM scales requires cosmological simulations. Moreover, doing so self-consistently, and capturing the effects of different phases of gas launched out of the disc initially, requires simulations that not only model CR transport and coupling but also magnetic fields, a multiphase ISM, SF, and stellar feedback processes (e.g. mechanical and radiative feedback). This explains why it has not been seen in most previous studies.

5.2 Observational implications

These modifications to outflows have a number of observational ramification, which fall into three categories:

(i) **Outflow Phase Structure:** As noted above, the CRs modify the phase structure (temperatures and densities) of outflows, as part of a general shift in the CGM phase structure when it is CR-pressure supported. A more detailed study of the observational effect of this change in CGM phase structure (including these outflows), and its consequences for UV and X-ray observations of CGM warm/hot gas, is the subject of Ji et al. (2020). Briefly, the overall lower temperatures, and higher gas densities in most of the CGM lead to an increase in the columns of warm absorbers (e.g. OVI) and decrease in hot absorbers (NeVIII) in MW-mass haloes. However, given the large scatter observed in the strength of these absorbers, it is difficult to unambiguously rule out either model at present, but this may be possible with larger statistical samples of simulations and observations.

(ii) **Outflow Kinematics:** A number of observations have suggested that there is a correlation between outflow velocity and galactocentric radius or impact parameter, of the form $v_r \propto r^{0.2-0.8}$ at radii $\sim$2–200 kpc (e.g. Steidel et al. 2010), which is suggestive of continuous outflow acceleration. Indeed, this is strikingly similar to the trend in the 'upper envelope' of v_r versus r seen in our Fig. 1 for our CR simulation. However, (a) the observational result remains controversial, (b) the *mean* v_r in the same simulation from Fig. 1 does not actually increase with radius in the same manner (see Fig. 4), despite acceleration of individual parcels (as they can reach lower terminal velocities at larger radii; see Fig. 6) so this clearly depends on how the 'velocity' measured is defined or weighted, and (c) a similar trend of increasing v_r with r can emerge naturally from thermal pressure-driven or even ballistic (decelerating) outflows, simply owing to the fact that if outflows are launched with a range of v_r, those with larger v_r reach larger r and do so more rapidly (Hopkins et al. 2013a). It is also the case that many observations have suggested a large fraction of outflow mass may be in 'slow' outflows (Heckman et al. 2015), qualitatively similar to the predictions in the CR-dominated models here. However, (a) absolute outflow rates across different gas phases are notoriously difficult to robustly measure and compare, (b) 'slow' outflows in particular are difficult to distinguish from turbulent or fountain motion within the halo (Muratov et al. 2017), and (c) once again, this is not a unique signature of CRs, as the same effect can arise from e.g. winds preferentially driven by stellar radiation pressure instead of mechanical (SNe) stellar feedback (Hopkins, Quataert & Murray 2012a; Zhang et al. 2018).

(iii) **Outflow Morphology:** Perhaps the most direct and robust testable prediction here is the effect of CRs on outflow morphology. A number of observational studies (primarily of Mg II and Fe II absorbers) have suggested outflows around $\sim L_*$ galaxies at $z \lesssim 2$ are preferentially bipolar and biconical (Kacprzak et al. 2011; Bouché et al. 2012; Kacprzak, Churchill & Nielsen 2012; Kornei et al. 2012; Rubin et al. 2014), in agreement with the CR-dominated halo predictions (Fig. 2). Even when non-CR feedback mechanisms can drive strong outflows in our simulations (e.g. in dwarfs, or high-redshift galaxies, or starburst systems), they are generally *not* strongly bipolar (and even when they are collimated they are not particularly well aligned with galactic discs; see Faucher-Giguere et al. 2015; Muratov et al. 2015; Hafen et al. 2017). However, some care is still needed: because the CR-driven outflows are 'slow' and the density in outflowing gas is relatively low, it is not obvious if the clear bipolar outflow structure seen in e.g. Fig. 2 actually translates to a clear observable trend of absorber equivalent width or velocity width as a function of polar angle. In subsequent work, we will forward-model the absorption-line profiles of MgII absorbers to quantitatively compare with these observations.

5.3 Caveats and future work

There are many interesting aspects of these simulations which remain to be explored. In future work, we plan to examine more detailed wind diagnostics, e.g. their phase, column density, and ionization-state distributions, which will allow us to directly compare to observational constraints on galactic outflows (and to make predictions for e.g. which observable phases/diagnostics should represent the bulk of the outflow material).

Given the deep physical uncertainties in CR transport in the CGM, this may represent the best path forward to constrain these models. Those uncertainties in CR physics will also be explored. We wish to strongly emphasize that we chose as our 'default' CR model here the implementation which had a near-maximal effect in Paper I. There and in Chan et al. (2019), we showed that a much lower CR diffusivity κ essentially eliminates all the effects here, as CRs are trapped too close to the galaxy (where their pressure is less important, and they lose energy rapidly to hadronic and Coulomb collisions), and leads to excessive γ-ray production (compared to observations). But if the diffusivity increases too rapidly in the CGM, or CRs de-couple from the stress tensor (e.g. 'slip' and stream out), then they will essentially do nothing to CGM gas (and such a scenario is theoretically at least plausible, and observationally allowed). So clearly it is important to develop and test more sophisticated CR transport models beyond the streaming + diffusion approximation here. Indeed, preliminary comparison with simulations including more complicated CR transport parametrizations motivated by extrinsic

turbulence or self-confinement theories in Hopkins et al. (2020a, b) suggests that while the CRs probably do not completely 'de-couple,' they do stream more rapidly at large galactocentric radii, weakening some of their effects in the CGM.

We have also emphasized above that the CR-driven outflows can reach enormous (>Mpc) scales: they may in fact go further and pollute a substantial fraction of the IGM, but we cannot continue our analysis much further before we start to approach the boundaries of the high-resolution 'zoom-in' region of these simulations (a few Mpc, at most). Large-volume simulations are clearly required to explore the potentially radical effects on even larger scales.

Finally, we have also focused our analysis on haloes with $z \sim 0$ masses $M_{\rm halo} \lesssim 10^{12}$–$10^{13}\,{\rm M}_{\odot}$. In Paper I, Su et al. (2019), and herein, we showed that in more massive haloes, or (equivalently) haloes which reach $\gtrsim 10^{12}\,{\rm M}_{\odot}$ at high redshifts $z \gtrsim 2$, the effects of CRs from SNe are weak, owing to a combination of lower $M_*/M_{\rm halo}$, higher halo/CGM gas pressure and column densities, and higher gas densities in the galaxy. However, such massive haloes have an additional, obvious source of CR feedback, namely AGN, which we have not included. This will be explored in companion papers such as Su et al. (2020) as well as future work focused on the broader question of the role of AGN feedback in such very massive haloes.

ACKNOWLEDGEMENTS

Support for PFH and co-authors was provided by an Alfred P. Sloan Research Fellowship, NSF Collaborative Research Grant #1715847 and CAREER grant #1455342, and NASA grants NNX15AT06G, JPL 1589742, and 17-ATP17-0214. CAFG was supported by NSF through grants AST-1517491, AST-1715216, and CAREER award AST-1652522, by NASA through grant 17-ATP17-0067, by STScI through grants HST-GO-14681.011, HST-GO-14268.022-A, and HST-AR-14293.001-A, and by a Cottrell Scholar Award from the Research Corporation for Science Advancement. DK was supported by NSF grant AST-1715101 and the Cottrell Scholar Award from the Research Corporation for Science Advancement. Numerical calculations were run on the Caltech compute cluster 'Wheeler,' allocations FTA-Hopkins supported by the NSF and TACC, and NASA HEC SMD-16-7592.

DATA AVAILABILITY STATEMENT

The data supporting the plots within this article are available on reasonable request to the corresponding author. A public version of the GIZMO code is available at http://www.tapir.caltech.edu/~phopkins/Site/GIZMO.html. Additional data including simulation snapshots, initial conditions, and derived data products are available at http://fire.northwestern.edu.

REFERENCES

Agertz O., Kravtsov A. V., Leitner S. N., Gnedin N. Y., 2013, ApJ, 770, 25
Amato E., Blasi P., 2018, Adv. Space Res., 62, 2731
Anglés-Alcázar D., Faucher-Giguère C.-A., Quataert E., Hopkins P. F., Feldmann R., Torrey P., Wetzel A., Kereš D., 2017, MNRAS, 472, L109
Blasi P., Amato E., 2012, J. Cosmol. Astropart. Phys., 1, 010
Bonaca A., Conroy C., Wetzel A., Hopkins P. F., Kereš D., 2017, ApJ, 845, 101
Booth C. M., Agertz O., Kravtsov A. V., Gnedin N. Y., 2013, ApJ, 777, L16
Bouché N., Hohensee W., Vargas R., Kacprzak G. G., Martin C. L., Cooke J., Churchill C. W., 2012, MNRAS, 426, 801
Boulares A., Cox D. P., 1990, ApJ, 365, 544
Braginskii S. I., 1965, Rev. Plasma Phys., 1, 205
Breitschwerdt D., McKenzie J. F., Voelk H. J., 1991, A&A, 245, 79
Breitschwerdt D., McKenzie J. F., Voelk H. J., 1993, A&A, 269, 54
Bryan G. L., Norman M. L., 1998, ApJ, 495, 80
Butsky I., Quinn T. R., 2018, ApJ, 868, 108
Butsky I. S., Fielding D. B., Hayward C. C., Hummels C. B., Quinn T. R., Werk J. K., 2020, ApJ, 903, 77
Chan T. K., Kereš D., Oñorbe J., Hopkins P. F., Muratov A. L., Faucher-Giguère C.-A., Quataert E., 2015, MNRAS, 454, 2981
Chan T. K., Keres D., Hopkins P. F., Quataert E., Su K. Y., Hayward C. C., Faucher-Giguere C. A., 2019, MNRAS, 488, 3716
Chen J., Bryan G. L., Salem M., 2016, MNRAS, 460, 3335
Colbrook M. J., Ma X., Hopkins P. F., Squire J., 2017, MNRAS, 467, 2421
Cole S., Lacey C. G., Baugh C. M., Frenk C. S., 2000, MNRAS, 319, 168
Cowie L. L., McKee C. F., 1977, ApJ, 211, 135
Croton D. J. et al., 2006, MNRAS, 365, 11
Cummings A. C. et al., 2016, ApJ, 831, 18
Dorfi E. A., Breitschwerdt D., 2012, A&A, 540, A77
El-Badry K. et al., 2018a, MNRAS, 477, 1536
El-Badry K. et al., 2018b, MNRAS, 473, 1930
El-Badry K. et al., 2018c, MNRAS, 480, 652
Escala I. et al., 2018, MNRAS, 474, 2194
Everett J. E., Zweibel E. G., Benjamin R. A., McCammon D., Rocks L., Gallagher III J. S., 2008, ApJ, 674, 258
Evoli C., Gaggero D., Vittino A., Di Bernardo G., Di Mauro M., Ligorini A., Ullio P., Grasso D., 2017, J. Cosmol. Astropart. Phys., 2, 015
Farber R., Ruszkowski M., Yang H.-Y. K., Zweibel E. G., 2018, ApJ, 856, 112
Faucher-Giguere C.-A., Hopkins P. F., Keres D., Muratov A. L., Quataert E., Murray N., 2015, MNRAS, 449, 987
Faucher-Giguère C.-A., Feldmann R., Quataert E., Kereš D., Hopkins P. F., Murray N., 2016, MNRAS, 461, L32
Fu L., Xia Z. Q., Shen Z. Q., 2017, MNRAS, 471, 1737
Gaggero D., Urbano A., Valli M., Ullio P., 2015, Phys. Rev. D, 91, 083012
Garrison-Kimmel S. et al., 2019, MNRAS, 487, 1380
Giacinti G., Kachelrie M., Semikoz D. V., 2018, J. Cosmol. Astropart. Phys., 7, 051
Ginzburg V. L., Ptuskin V. S., 1985, Astrophys. Space Phys. Rev., 4, 161
Greene J. E., Zakamska N. L., Ho L. C., Barth A. J., 2011, ApJ, 732, 9
Guo F., Oh S. P., 2008, MNRAS, 384, 251
Guo Y.-Q., Tian Z., Jin C., 2016, ApJ, 819, 54
Hafen Z. et al., 2017, MNRAS, 469, 2292
Hafen Z. et al., 2019, MNRAS, 488, 1248
Hafen Z. et al., 2020, MNRAS, 494, 3581
Hahn O., Abel T., 2011, MNRAS, 415, 2101
Heckman T. M., Lehnert M. D., Strickland D. K., Armus L., 2000, ApJS, 129, 493
Heckman T. M., Alexandroff R. M., Borthakur S., Overzier R., Leitherer C., 2015, ApJ, 809, 147
Hernquist L., 1990, ApJ, 356, 359
Holman G. D., Ionson J. A., Scott J. S., 1979, ApJ, 228, 576
Hopkins P. F., 2015, MNRAS, 450, 53
Hopkins P. F., 2016, MNRAS, 462, 576
Hopkins P. F., 2017, MNRAS, 466, 3387
Hopkins P. F., Hernquist L., 2006, ApJS, 166, 1
Hopkins P. F., Hernquist L., 2009, ApJ, 694, 599
Hopkins P. F., Raives M. J., 2016, MNRAS, 455, 51
Hopkins P. F., Hernquist L., Cox T. J., Di Matteo T., Robertson B., Springel V., 2006, ApJS, 163, 1
Hopkins P. F., Quataert E., Murray N., 2011, MNRAS, 417, 950
Hopkins P. F., Quataert E., Murray N., 2012a, MNRAS, 421, 3522
Hopkins P. F., Quataert E., Murray N., 2012b, MNRAS, 421, 3488
Hopkins P. F., Kereš D., Murray N., Hernquist L., Narayanan D., Hayward C. C., 2013a, MNRAS, 433, 78
Hopkins P. F., Narayanan D., Murray N., 2013b, MNRAS, 432, 2647
Hopkins P. F., Keres D., Onorbe J., Faucher-Giguere C.-A., Quataert E., Murray N., Bullock J. S., 2014, MNRAS, 445, 581

Hopkins P. F. et al., 2018a, MNRAS, 480, 800
Hopkins P. F. et al., 2018b, MNRAS, 477, 1578
Hopkins P. F., Chan T. K., Squire J., Quataert E., Ji S., Keres D., Faucher-Giguere C.-A., 2020a, preprint (arXiv:2004.02897)
Hopkins P. F., Squire J., Chan T. K., Quataert E., Ji S., Keres D., Faucher-Giguere C.-A., 2020b, MNRAS, in press, preprint (arXiv:2002.06211)
Hopkins P. F., Grudic M. Y., Wetzel A. R., Keres D., Faucher-Giguere C.-A., Ma X., Murray N., Butcher N., 2020c, MNRAS, 491, 3702
Hopkins P. F. et al., 2020d, MNRAS, 492, 3465 (Paper I)
Ipavich F. M., 1975, ApJ, 196, 107
Ji S. et al., 2020, MNRAS, 496, 4221
Jóhannesson G. et al., 2016, ApJ, 824, 16
Jubelgas M., Springel V., Enßlin T., Pfrommer C., 2008, A&A, 481, 33
Kacprzak G. G., Churchill C. W., Evans J. L., Murphy M. T., Steidel C. C., 2011, MNRAS, 416, 3118
Kacprzak G. G., Churchill C. W., Nielsen N. M., 2012, ApJ, 760, L7
Kannan R., Stinson G. S., Macciò A. V., Brook C., Weinmann S. M., Wadsley J., Couchman H. M. P., 2014, MNRAS, 437, 3529
Katz N., Weinberg D. H., Hernquist L., 1996, ApJS, 105, 19
Kereš D., Katz N., Davé R., Fardal M., Weinberg D. H., 2009, MNRAS, 396, 2332
Komarov S., Schekochihin A. A., Churazov E., Spitkovsky A., 2018, J. Plasma Phys., 84, 905840305
Kormendy J., Bender R., Cornell M. E., 2011, Nature, 469, 374
Kornei K. A., Shapley A. E., Martin C. L., Coil A. L., Lotz J. M., Schiminovich D., Bundy K., Noeske K. G., 2012, ApJ, 758, 135
Korsmeier M., Cuoco A., 2016, Phys. Rev. D, 94, 123019
Krongold Y., Nicastro F., Elvis M., Brickhouse N., Binette L., Mathur S., Jiménez-Bailón E., 2007, ApJ, 659, 1022
Kroupa P., 2001, MNRAS, 322, 231
Krumholz M. R., Gnedin N. Y., 2011, ApJ, 729, 36
Kulsrud R. M., 2005, Plasma Physics for Astrophysics. Princeton Univ. Press, Princeton, NJ
Kulsrud R., Pearce W. P., 1969, ApJ, 156, 445
Lacki B. C., Thompson T. A., Quataert E., Loeb A., Waxman E., 2011, ApJ, 734, 107
Leitherer C. et al., 1999, ApJS, 123, 3
Lopez L. A., Auchettl K., Linden T., Bolatto A. D., Thompson T. A., Ramirez-Ruiz E., 2018, ApJ, 867, 44
McKenzie J. F., Voelk H. J., 1982, A&A, 116, 191
Ma X., Hopkins P. F., Faucher-Giguère C.-A., Zolman N., Muratov A. L., Kereš D., Quataert E., 2016, MNRAS, 456, 2140
Ma X., Hopkins P. F., Feldmann R., Torrey P., Faucher-Giguère C.-A., Kereš D., 2017a, MNRAS, 466, 4780
Ma X., Hopkins P. F., Wetzel A. R., Kirby E. N., Anglés-Alcázar D., Faucher-Giguère C.-A., Kereš D., Quataert E., 2017b, MNRAS, 467, 2430
Ma X. et al., 2018, MNRAS, 478, 1694
Mannheim K., Schlickeiser R., 1994, A&A, 286, 983
Mao S. A., Ostriker E. C., 2018, ApJ, 854, 89
Martin C. L., 1999, ApJ, 513, 156
Martin C. L., Scannapieco E., Ellison S. L., Hennawi J. F., Djorgovski S. G., Fournier A. P., 2010, ApJ, 721, 174
Muratov A. L., Kereš D., Faucher-Giguère C.-A., Hopkins P. F., Quataert E., Murray N., 2015, MNRAS, 454, 2691
Muratov A. L. et al., 2017, MNRAS, 468, 4170
Oñorbe J., Garrison-Kimmel S., Maller A. H., Bullock J. S., Rocha M., Hahn O., 2014, MNRAS, 437, 1894
Oñorbe J., Boylan-Kolchin M., Bullock J. S., Hopkins P. F., Kereš D., Faucher-Giguère C.-A., Quataert E., Murray N., 2015, MNRAS, 454, 2092
Pettini M., Madau P., Bolte M., Prochaska J. X., Ellison S. L., Fan X., 2003, ApJ, 594, 695
Roškar R., Teyssier R., Agertz O., Wetzstein M., Moore B., 2014, MNRAS, 444, 2837
Rubin K. H. R., Prochaska J. X., Koo D. C., Phillips A. C., Martin C. L., Winstrom L. O., 2014, ApJ, 794, 156
Ruszkowski M., Yang H.-Y. K., Zweibel E., 2017, ApJ, 834, 208
Salem M., Bryan G. L., 2014, MNRAS, 437, 3312
Sanderson R. E. et al., 2018, ApJ, 869, 12
Sato T., Martin C. L., Noeske K. G., Koo D. C., Lotz J. M., 2009, ApJ, 696, 214
Simpson C. M., Pakmor R., Marinacci F., Pfrommer C., Springel V., Glover S. C. O., Clark P. C., Smith R. J., 2016, ApJ, 827, L29
Skilling J., 1971, ApJ, 170, 265
Socrates A., Davis S. W., Ramirez-Ruiz E., 2008, ApJ, 687, 202
Somerville R. S., Primack J. R., 1999, MNRAS, 310, 1087
Songaila A., 2005, AJ, 130, 1996
Sparre M., Hayward C. C., Feldmann R., Faucher-Giguère C.-A., Muratov A. L., Kereš D., Hopkins P. F., 2017, MNRAS, 466, 88
Spitzer L., Härm R., 1953, Phys. Rev., 89, 977
Springel V., Hernquist L., 2003, MNRAS, 339, 312
Squire J., Kunz M. W., Quataert E., Schekochihin A. A., 2017a, Phys. Rev. Lett., 119, 155101
Squire J., Quataert E., Kunz M. W., 2017b, J. Plasma Phys., 83, 905830613
Squire J., Schekochihin A. A., Quataert E., 2017c, New J. Phys., 19, 055005
Steidel C. C., Erb D. K., Shapley A. E., Pettini M., Reddy N., Bogosavljević M., Rudie G. C., Rakic O., 2010, ApJ, 717, 289
Stern J., Fielding D., Faucher-Giguère C.-A., Quataert E., 2019, MNRAS, 488, 2549
Su K.-Y., Hopkins P. F., Hayward C. C., Faucher-Giguère C.-A., Kereš D., Ma X., Robles V. H., 2017, MNRAS, 471, 144
Su K.-Y. et al., 2019, MNRAS, 487, 4393
Su K.-Y. et al., 2020, MNRAS, 491, 1190
Tasker E. J., 2011, ApJ, 730, 11
Tremonti C. A. et al., 2004, ApJ, 613, 898
Vladimirov A. E., Jóhannesson G., Moskalenko I. V., Porter T. A., 2012, ApJ, 752, 68
Weiner B. J. et al., 2009, ApJ, 692, 187
Wentzel D. G., 1968, ApJ, 152, 987
Wheeler C. et al., 2017, MNRAS, 465, 2420
Wiener J., Zweibel E. G., Oh S. P., 2013, ApJ, 767, 87
Wise J. H., Abel T., Turk M. J., Norman M. L., Smith B. D., 2012, MNRAS, 427, 311
Yan H., Lazarian A., 2008, ApJ, 673, 942
Zhang D., Davis S. W., Jiang Y.-F., Stone J. M., 2018, ApJ, 854, 110
Zirakashvili V. N., Breitschwerdt D., Ptuskin V. S., Voelk H. J., 1996, A&A, 311, 113

APPENDIX A: ADDITIONAL VELOCITY FIELD IMAGES

Here, we include some additional detailed images of the galaxy velocity fields, in the style of Fig. 2.

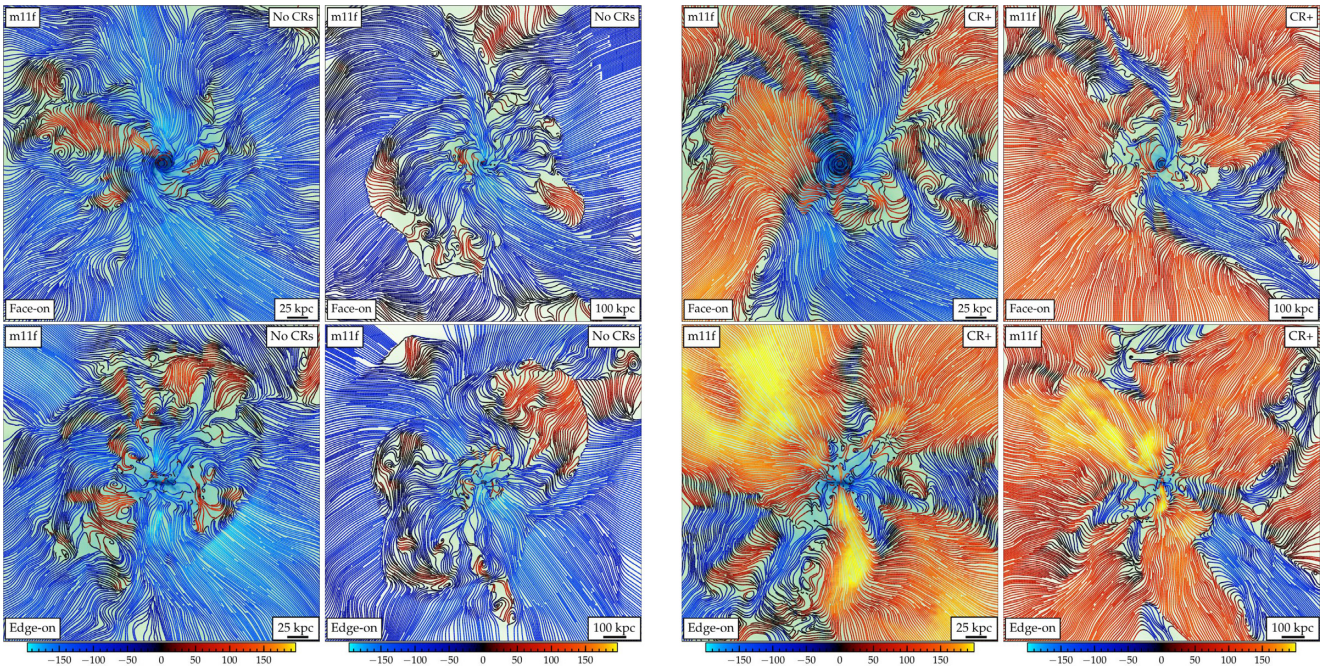

Figure A1. As Fig. 14, for **m11f**. The galaxy is somewhat less massive, but still has an SFR strongly suppressed by CRs and a CR-dominated halo in the 'CR+' run. The lower halo mass (more rapid cooling) means the virial shock is somewhat less sharp in the 'No CRs' run (compared to the **m12** runs), but we still see a similar qualitative change in behaviour out to $\gg R_{\rm vir}$.

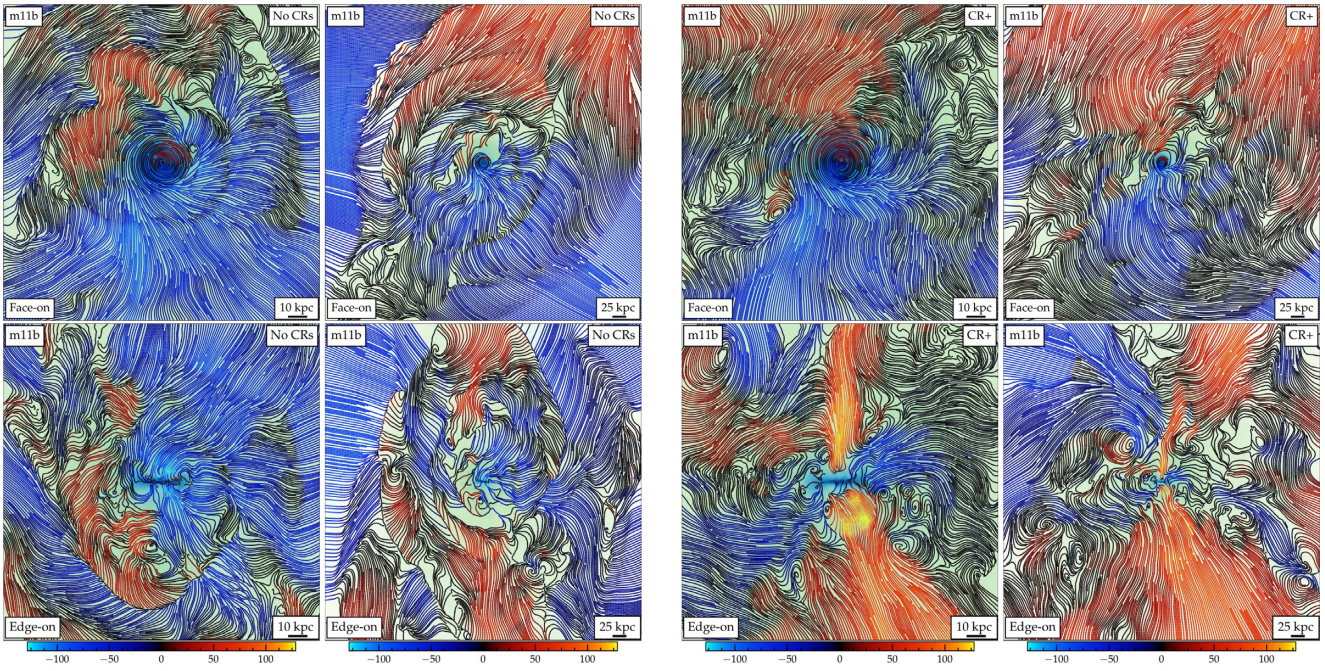

Figure A2. As Fig. 14, for **m11b**. This galaxy is low enough in mass ($M_* \sim 10^8\,{\rm M}_\odot$, $M_{\rm halo} \sim 4\times10^{10}\,{\rm M}_\odot$) such that the effect of CRs on galaxy properties is significantly weaker. However, significant effects of CRs on CGM/IGM scales $\sim$ 1–4 $R_{\rm vir}$ are still apparent. Edge-on, the 'No CRs' run features shocks and a quasi-spherical/isotropic and turbulent flow structure, while the 'CR+' run exhibits a bipolar structure (albeit with less volume-filling outflow). Face-on, the 'No CRs' run exhibits a clear series of concentric shocks towards $R_{\rm vir}$, but these are absent in the CR run.

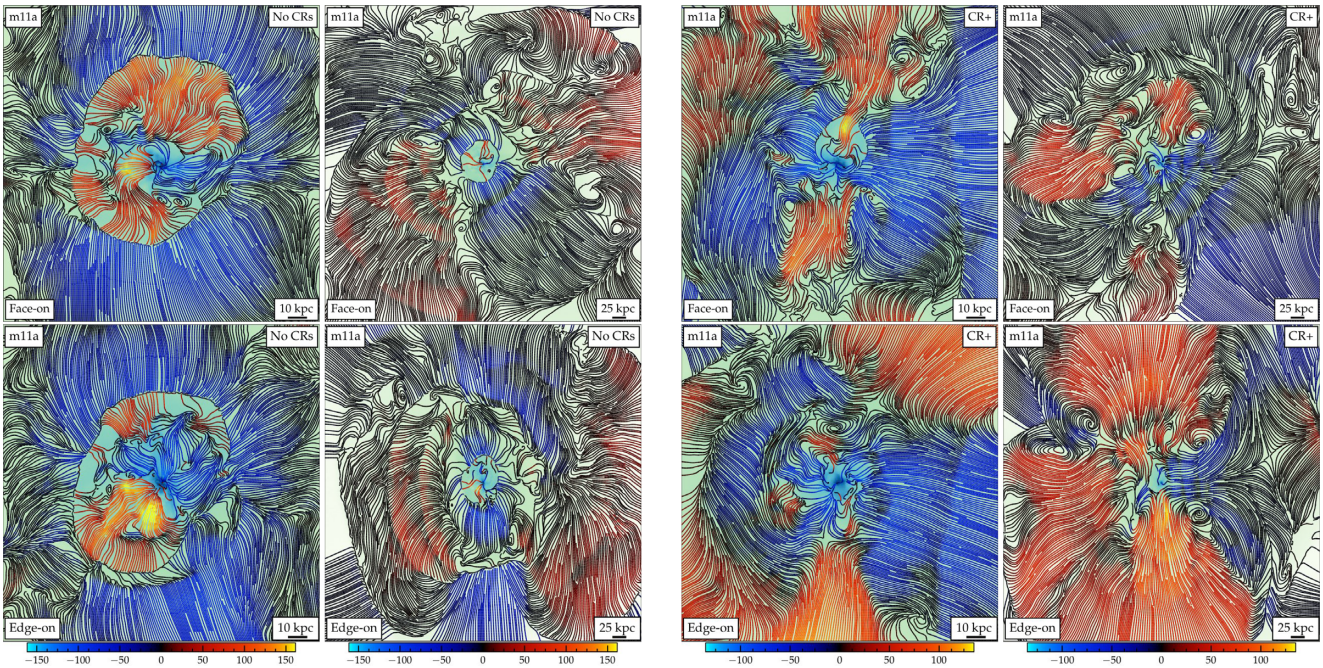

Figure A3. As Fig. 14, for **m11a**. Like **m11b**, the low mass ($M_* \sim 5 \times 10^7\,M_\odot$, $M_{\rm halo} \sim 4 \times 10^{10}\,M_\odot$) means CRs have relatively modest effects, but some differences on scales $\sim$ 1–4 $R_{\rm vir}$ are still evident. The 'No CRs' run is close to spherically symmetric (with a clear shock where disc outflows meet accretion at $\sim 0.5\,R_{\rm vir}$), and weak inflow shocks at larger radii. The 'CR+' run shows a large-scale bipolar outflow that does not extend to the disc but has a 'base' at $\sim$ 30–50 kpc from the disc, reflecting collimation and acceleration by the CGM.

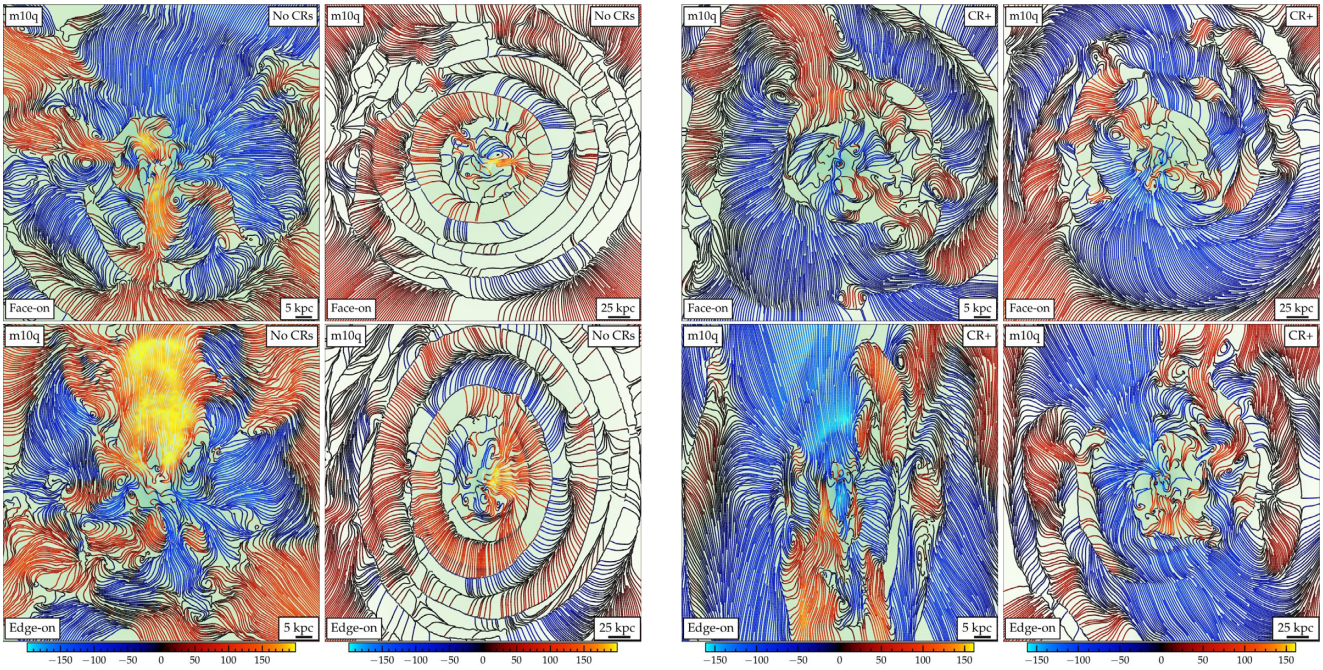

Figure A4. As Fig. 14, for **m10q**. By this mass ($M_{\rm halo} \sim 10^{10}\,M_\odot$), the contribution of CRs to the halo pressure is quite weak (Fig. 8), and it is difficult to discern an obvious systematic change to the inflow/outflow structure around the galaxy – the 'No CRs' run actually has a more obvious strong outflow at this particular time, owing to a recent burst of SF.

This paper has been typeset from a TEX/LATEX file prepared by the author.